RAD52 prevents accumulation of Polα-dependent replication gaps at perturbed replication forks in human cells

[1 #] Ludovica Di Biagi, [1 *] Giorgia Marozzi,[1 *] Eva Malacaria, [3] Masayoshi Honda, [1 §] Francesca Antonella Aiello, [1] Pasquale Valenzisi, [3] Maria Spies, [1] Annapaola Franchitto and Pietro Pichierri [1,2 §]

1 Mechanisms, Biomarkers and Models Section, Genome Stability Group, Department of Environment and Health, Istituto Superiore di Sanità - Viale Regina Elena 299, 00161 Rome (Italy)
2 Istituto Nazionale Biostrutture e Biosistemi - Roma Area Research - Via delle Medaglie d'Oro 305, 00136 Rome (Italy)
3 Department of Biochemistry and Molecular Biology, University of Iowa Carver College of Medicine, 51 Newton Road, Iowa City, IA 52242 (USA)

present address:
§ present address: Department of Hematology/Oncology, Cell and Gene Therapy, Bambino Gesù Children's Hospital, IRCCS, Rome (Italy)

* GM and EM equally contributed

§ Author to whom correspondence should be addressed:

Pietro Pichierri
Tel. +39 0649902355
Fax +39 0660513138
pietro.pichierri@iss.it

Running title: RAD52 and replication gaps

ABSTRACT

Replication gaps can arise as a consequence of perturbed DNA replication and their accumulation might undermine the stability of the genome. Loss of RAD52, a protein involved in the regulation of fork reversal, promotes accumulation of parental ssDNA gaps during replication perturbation. Here, we demonstrate that this is due to the engagement of Polα downstream of the extensive degradation of perturbed replication forks after their reversal, and is not dependent on PrimPol. Polα is hyper-recruited at parental ssDNA in the absence of RAD52, and this recruitment is dependent on fork reversal enzymes and RAD51. Of note, we report that the interaction between Polα and RAD51 is stimulated by RAD52 inhibition, and Polα-dependent gap accumulation requires nucleation of RAD51 suggesting that it occurs downstream strand invasion. Altogether, our data indicate that RAD51-Polα-dependent repriming is essential to promote fork restart and limit DNA damage accumulation when RAD52 function is disabled.

INTRODUCTION

The response to perturbed replication fork progression is crucial to prevent accumulation of unreplicated DNA regions, DNA damage and genomic rearrangements [1–4]. For this reason, cells evolved multiple mechanisms of protection that deal with impaired replication fork progression and replication stress [3,5,6]. A crucial step in this process is represented by the DNA remodelling occurring at perturbed or stalled replication forks. Fork remodelling involves the reannealing of the two nascent strands promoted by regression of the replication fork structures producing a four-way DNA intermediate called reversed fork (RF) [7]. This reaction has been first discovered in bacteria where it is catalysed by RecG while, in human cells, involves multiple factors including SMARCAL1, ZRANB3 and the homologous recombination protein RAD51 [6,8,9]. If on one hand the RF contributes to protect nascent ssDNA, on the other hand it produces a DNA end that can be attacked by nucleases. Thus, the RF extruded strand is protected by unscheduled and extensive degradation by BRCA2, RAD51 and other proteins acting as “barriers” against the action of MRE11 and EXO1 [5,10–12]. Pathological DNA transactions at replication forks is also counteracted by proteins that regulate fork remodelling, such as ATR or RADX [13,14]. In addition, we have recently uncovered a role for RAD52 in preventing fork degradation by regulating the extent of SMARCAL1 having access to the DNA replication fork [15]. Since the reversed fork can be also a target for exo- or endonucleases [3,5], cells balance its usage with other mechanism granting continuation of DNA synthesis. Recently, it has been reported that replication fork reversal and repriming act as parallel “fork recovery” pathways: too limited fork reversal upregulates repriming and vice versa [16–18]. In yeast, repriming under perturbed replication involves the Polα primase but recent reports indicated that a specialised Primase-Polymerase, PrimPol, takes over in humans [19–22].

Repriming at perturbed replication forks leads to accumulation of ssDNA gaps that needs to be subsequently repaired to prevent accumulation of unreplicated DNA in mitosis [23,24]. Intriguingly, abrogation of RAD52 function stimulates formation of parental ssDNA although it does not overtly affect ability of fork to restart after stalling [15].

Here, we used multiple cell biology techniques and cell models to investigate if loss of RAD52 function could affect the repriming in response to perturbed replication. We show that loss of RAD52 function stimulates the accumulation of parental ssDNA gaps and that those gaps are not dependent on PrimPol but rather are dependent on Polα. In the absence of a functional RAD52, origin-independent Polα recruitment at DNA is stimulated.

Such origin-independent Polα recruitment occurs downstream fork reversal and degradation, and is mechanistically-linked to inability to induce MUS81-dependent DSBs at the degraded reversed forks. Intriguingly, the recruitment of Polα licensed by RAD52 inactivity requires RAD51 nucleofilaments and involves binding with RAD51 itself. Under these conditions, engagement of this Polα-mediated repriming is instrumental in ensuring maximal fork recovery and DNA damage avoidance.

Therefore, our results uncover a novel mechanism of repriming granting fork recovery and protecting from genome instability engaged when aberrant or partial DNA transactions occur at perturbed replication forks.

RESULTS

RAD52 prevents formation of gaps at perturbed replication forks.

Perturbed replication forks are extensively degraded in the absence of RAD52; however, a large part of them retains the ability to resume DNA synthesis [15]. Two main pathways are used to resume degraded DNA replication forks: recombination and repriming [3,24,25]. Since RAD52 inactivation should prevent DSB formation at degraded forks and subsequent break-induced replication [11], we analysed whether replication fork recovery in the absence of active RAD52 involved repriming events. To this end, we monitored the exposure of ssDNA on the parental strand, which may derive from repriming events, in cells treated with the RAD52 inhibitor ECG (RAD52i; [26]) and 2mM HU after labelling DNA for 24h with Iododeoxyuridine (IdU) (Figure 1A). As inhibition of RAD52 did not induce parental ssDNA accumulation during treatment with 2mM HU [15], parental ssDNA was analysed at multiple recovery times by a native IdU detection [27] (Figure 1A). We found that parental ssDNA can be detected in RAD52-proficient and RAD52-deficient cells after 2h of recovery, however, parental ssDNA was significantly higher in cells inhibited of RAD52 after 4h of recovery and persisted also at 18h of recovery.

Consistent with the results obtained with the RAD52i, stable depletion of RAD52 using RNAi [15] also led to high and persistent levels of parental ssDNA during recovery from replication arrest (Supplementary Figure 1A). To exclude that parental ssDNA might derive from extensive MRE11-mediated fork degradation and to validate our data in a different background, we evaluated the presence of ssDNA during recovery in U2OS cells treated with RAD52i alone or in combination with the MRE11 inhibitor MIRIN. As shown in Figure 1B, the inhibition of MRE11 during replication arrest did not have much effect on parental ssDNA levels in RAD52-deficient cells at 2h of recovery, although it reduced the level of parental ssDNA at 4h of recovery. Subsequently, we analyzed the presence of parental ssDNA in cells treated with 0.5mM HU. This dose is commonly used to evaluate ssDNA gaps as it slows down replication without causing complete stalling [28]. In wild-type U2OS cells treated with 0.5mM HU, some exposure of parental ssDNA was detected. However, when RAD52 was inhibited (Figure 1C) or stably depleted (Supplementary Figure 1B), the amount of parental ssDNA detected by IF greatly increased, especially at 4 hours of treatment. Treatment with MIRIN did not significantly affect parental ssDNA exposure at 2h of treatment with 0.5mM HU even if a minor reduction was observed at 4h of treatment (Figure 1C). As shown by our previous studies [15], neither acute RAD52 inhibition nor

RNAi-mediated downregulation affected the number of S-phase cells or IdU incorporation, ruling-out the possibility that the effect of RAD52 inhibition on parental ssDNA exposure in response to perturbed replication is due to differences in S-phase cell numbers or IdU incorporation (Supplementary Figure 2A-E).

To demonstrate that the elevated levels of parental ssDNA detected in the absence of RAD52 correlated with the presence of replicative gaps, we performed the S1 DNA fiber assay [29]. We pulse-labelled cells with CldU followed by labelling with IdU and treatment with 0.5mM HU, in the presence or not of the RAD52i (see scheme in Figure 1D). As previously shown [15], RAD52 inhibition did not affect fork progression rates per se (Supplementary Figure 3). After treatment, cells were exposed to S1 nuclease to cut regions of ssDNA before obtaining DNA fibers. Thus, while intact replication tracts are expected to have an IdU/CldU ratio greater than 1, since IdU can be incorporated, even if at a reduced pace, during the 4-hour treatment with 0.5mM HU, gap-containing replication tracts are expected to be shorter after treatment with S1 nuclease, leading to an IdU/CldU ratio less than 1. Following treatment with 0.5mM HU, cells inhibited of RAD52 showed an IdU/CldU ratio that was comparable to that of non-inhibited cells (Figure 1D). Treatment with S1 nuclease significantly reduced the IdU/CldU ratio in cells inhibited of RAD52 but not significantly in wild-type cells (Figure 1D), confirming that RAD52 deficiency induces the accumulation of parental DNA gaps at perturbed replication forks.

These results demonstrate that upon replication perturbation, the inhibition or depletion of RAD52 leads to the formation of gaps in parental DNA.

Inhibition of RAD52 stimulates Polα-dependent gaps.

The accumulation of gaps at perturbed replication forks in BRCA-deficient cells is attributed to a defect in regulating the metabolism of Okazaki fragments and is correlated with PrimPol-mediated repriming [16,30,31]. Thus, we used wild-type or PrimPol KO MRC5SV40 cells [32] to test if gaps might derive from the repriming activity of PrimPol also in cells inhibited of RAD52. To analyse gaps, we performed the DNA fiber S1 assay in cells treated with 0.5mM HU. RAD52 mock-inhibited cells (WT) did not experience a significant accumulation of DNA gaps since the IdU/CldU ratios were not statistically different compared with the same cells treated with the S1 nuclease (Figure 2A). PrimPol KO cells showed relatively longer IdU tracts in 0.5mM HU, however, loss of PrimPol did not induce any significant rescue in the IdU/CldU ratios compared to the wild-type (Figure 2A). Inhibition of RAD52, as expected, resulted in accumulation of DNA gaps following

replication perturbation as shown by the ability of S1 to shorten the IdU tract and determine IdU/CldU ratios < 1 (Figure 2A). Interestingly, in cells inhibited of RAD52, S1 nuclease treatment reduced the IdU/CldU ratio following replication perturbation even in the absence of PrimPol (Figure 2A), indicating that gaps are PrimPol-independent. We hypothesized that if PrimPol was not involved in repriming, it would not be recruited to the replication fork when RAD52 was inhibited. Thus, we decided to investigate the recruitment of PrimPol at parental ssDNA following fork arrest by *in situ* PLA [15,27] (Figure 2B). Since none of the available anti-PrimPol antibodies were suitable for PLA, we added GFP-PrimPol back into PrimPol KO MRC5SV40 cells (Figure 2B). In untreated cells, a low level of PrimPol was found to be associated with parental ssDNA, regardless of RAD52 function (Figure 2B). Surprisingly, even though no DNA gaps were detected in mock-inhibited cells, treatment with HU significantly increased the association of PrimPol with parental ssDNA in these cells. However, the recruitment of GFP-PrimPol to parental DNA was not stimulated by HU when RAD52 was inhibited (Figure 2B). To confirm our PLA data, we performed chromatin fractionation. Consistent with the PLA data, PrimPol KO cells accumulated GFP-PrimPol in chromatin in the absence of the RAD52 inhibitor, while the normalized amount of GFP-PrimPol did not increase comparably in the presence of the inhibitor following HU treatment, especially at 2h (Figure 2C). By contrast and consistent with recent data [17], depletion of SMARCAL1 led to an increase of PrimPol-dependent replicative gaps in doxycycline-inducible shSMARCAL1 U2OS cells compared to control-depleted cells (Supplementary Figure 4A,B).

Having shown that replicative gaps accumulating following loss of RAD52 function are not PrimPol-dependent, we examined their dependency from Polα. Indeed, in yeast, replication stress-associated gaps are produced by Polα when fork remodelling is hampered [20]. We first investigated the recruitment of Polα at parental ssDNA by *in situ* IdU-Polα PLA (Figure 2D). Recruitment of Polα to parental ssDNA was stimulated by inhibition of RAD52 already under unperturbed replication and, even more, after treatment with HU, although replication fork arrest increased the presence of Polα at parental ssDNA also in wild-type cells (Figure 2D and Supplementary Figure 5). Since inhibiting RAD52 did not affect the number of cells in S-phase or the incorporation of IdU, the observed differences are genuine (see Supplementary Figure 2). Combining *in situ* IdU-Polα PLA with EdU immunofluorescence to label S-phase cells, we confirmed that the large part of de-novo localisation of Polα to parental ssDNA observed when RAD52 is inhibited occurs in EdU-positive cells (Supplementary Figure 6A-B). Of note, a minority of PLA spots were

found also in EdU-negative cells. However, EdU-negative cells displayed few PLA spots – typically seven or less – and this unexpected localisation was not affected by RAD52 inhibition, although seems to be more represented in HU-treated cells (Supplementary Figure 6A). Increased recruitment of Polα might be correlated with ancillary origin firing stimulated by replication fork arrest in the RAD52-deficient background [15]. To assess if increased Polα recruitment might depend on new origin firing, we suppressed their activation by treating cells with the CDC7 inhibitor XL413 (CDC7i) during HU. Interestingly, treatment with the CDC7i barely affected the low level of Polα association with ssDNA in mock-inhibited cells and, most importantly, did not reduce the increased association of POLA1 with ssDNA when RAD52 is inhibited (Supplementary Figure 7A). Consistent with PLA, chromatin fractionation confirmed the CDC7i-independent recruitment of POLA1 in RAD52i-treated cells in response to replication arrest (Supplementary Figure 7B), further excluding that de-novo Polα recruitment depends on origin firing in HU.

During unchallenged replication and in response to DNA damage, Polα is recruited at the replisome by Ctf-4/AND-1 [20,33]. Thus, we analysed if replication arrest-dependent recruitment of Polα at parental ssDNA in the absence of RAD52 was similarly dependent on the presence of AND-1. To this end, we depleted AND-1 in RAD52i-treated cells and assessed the interaction between Polα and DNA by PLA in response to replication perturbation (Supplementary Figure 7C and D). As repeatedly observed in other experiments, inhibition of RAD52 greatly increased the amount of Polα detected at ssDNA after replication perturbation. Depletion of AND-1 slightly reduced the number of ssDNA-Polα spots in RAD52-proficent cells but reset the number of PLA spot to the level of non-inhibited cells when combined with RAD52i (Supplementary Figure 7D).

Since inhibition of RAD52 stimulated the recruitment of Polα over that of PrimPol, we next analysed if inhibition of Polα might revert the excess of parental ssDNA in RAD52i-treated cells.

Treatment with a Polα inhibitor (ST1926; POLA1i) dramatically increases ssDNA at fork and eventually blocks replication [34]. Thus, we decided to titrate the amount of inhibitor against EdU incorporation and select a concentration that does not impact significantly on DNA synthesis (Supplementary Figure 8). While the doses of the inhibitor used to block Polα [34] suppressed EdU incorporation, the 0.3μM dose only minimally reduced EdU incorporation in terms of number of positive cells and EdU intensity. Thus, we wondered if this low concentration of POLA1i might be useful to impact more on the additional pool of protein engaged in the absence of RAD52 at perturbed replication forks. To this end, we

evaluated the exposure of parental ssDNA at 0.5mM HU by adding the POLA1i during HU (Figure 2E). As a control, we combined the low-dose of POLA1i and the CDC7i to pinpoint only the origin-independent function of Polα. As a positive control for ssDNA accumulation, wild-type cells were treated with 3μM of POLA1i.

Consistent with an involvement of Polα in the exposure of parental ssDNA when RAD52 is inhibited, treatment with the low-dose of POLAi greatly decreased the accumulation of parental ssDNA stimulated in the presence of the RAD52i, while only minimally reduced exposure of ssDNA in wild-type cells (Figure 2E). Combined treatment with the CDC7i and 0.3μM POLA1i did no further reduce parental ssDNA during HU treatment of RAD52-inhibited cells (Figure 2E). As expected, the high dose of POLA1i (3μM) led to the exposure of a huge amount of ssDNA in unperturbed cells (Figure 2E). These results indicate that the treatment with a low-dose of POLA1i during perturbed replication can be used to target de-novo recruitment of Polα in RAD52-inhibited cells and further confirm that this pool of Polα engaged upon replication perturbation is not working at new origins.

To further assess the role of Polα in the formation of replicative gaps when RAD52 is inhibited, we performed the S1 DNA fiber assay in wild-type or PrimPol KO MRC5SV40 cells, treated or not with the low-dose of POLA1i. Our expectation was to find PrimPol-dependent gaps in RAD52-proficient cells and POLA1i-sensitive gaps in cells inhibited of RAD52. Compared with cells treated with only HU, the inhibition of POLA1 did not reduce the IdU/CldU ratio in S1-treated fibers in wild-type cells (Figure 2F). In PrimPol KO cells, inhibition of POLA1 reduced the IdU/CldU ratio, possibly indicating that gaps were introduced but independently on the PrimPol or Polα function (Figure 2F). Compared with mock-inhibited wild-type cells, inhibition of RAD52 reduced the IdU/CldU ratio of the S1-treated DNA fibers and the tract length ratio was not recovered in PrimPol KO cells (Figure 2F). In contrast, the low-dose of POLA1i increased significantly the IdU/CldU ratio in S1 DNA fibers from RAD52i-treated wild-type cells and, in a similar extent, also in the PrimPol KO (Figure 2F).

Collectively, these results indicate that inhibition of RAD52 stimulates an origin-independent recruitment of Polα that is linked to accumulation of replicative gaps through a Polα-dependent but PrimPol-independent mechanism.

Recruitment of Polα at perturbed replication forks depends on fork reversal.

Since loss or inhibition of RAD52 stimulates degradation of reversed forks [15], we next investigated if stimulation of Polα recruitment could occur downstream fork reversal. Thus,

we analysed association of Polα with parental ssDNA by PLA in MRC5SV40 cells stably expressing a doxycycline-regulated shSMARCAL1 cassette (Supplementary Figure 9; [35]). Depletion of SMARCAL1 greatly reduced the recruitment of Polα at parental ssDNA stimulated by RAD52 inhibition under perturbed replication (Figure 3A). Of note, downregulation of SMARCAL1 decreased the number of PLA spots also in the absence of RAD52i. Consistent with PLA data, depletion of SMARCAL1 reduced the amount of POLA1 detected in chromatin fractions from cells treated with the RAD52i (Figure 3B). The inhibition of RAD52 leads to fork degradation as it unleashes recruitment of fork reversal enzymes [15]. A similar condition can be obtained by overexpressing SMARCAL1 [13]. Interestingly, when we induced a strong SMARCAL1 overexpression through the piggybac system in U2OS cells (Supplementary Figure 10A) we failed to detect an increase of Polα-parental ssDNA PLA spots over the non-overexpressing cells and, unexpectedly, the number of PLA signals decreased upon SMARCAL1 overexpression (Figure S10B). This result was not the consequence of DSBs, which are stimulated by uncontrolled fork reversal [13] since it was not affected by depletion of MUS81, the nuclease contributing to DSBs formation in this conditions [13] (Supplementary Figure 10A,B). Thus, engagement of Polα at perturbed forks when RAD52 is inhibited is not just a consequence of unrestrained fork reversal or breakage at unreversed forks.

Thus, we then investigated if enhanced recruitment of Polα taking place downstream fork reversal when RAD52 is inhibited was functionally related to the nascent-strand degradation that occurs at reversed forks in the absence of RAD52 [15]. Thus, we blocked fork degradation by exposing cells to the MRE11 inhibitor Mirin, alone or in combination with the RAD52i, and then analysed the presence of POLA1 at parental ssDNA by PLA (Figure 3C). In cells where RAD52 was inhibited, the hyper-recruitment of POLA1 at ssDNA was significantly decreased by Mirin, but not completely eliminated. These results suggest that the hyper-recruitment of Polα occurring when RAD52 is inhibited is mostly a consequence of MRE11-dependent degradation at remodelled forks [15]. To investigate if stimulation of Polα recruitment might represent a general response to the degradation of reversed forks, we analysed the presence of Polα at parental ssDNA by performing PLA experiments in BRCA2-depleted cells; the prototypical model of fork deprotection and MRE11-dependent degradation. In response to replication fork arrest, the association of POLA1 with parental ssDNA was not increased by BRCA2 depletion as compared with mock-depleted cells and, most importantly, was not affected by preventing fork degradation with Mirin (Figure 3D). In contrast, recruitment at parental ssDNA of

transiently-expressed GFP-tagged PrimPol was significantly stimulated by BRCA2 downregulation as compared to the wild-type or RAD52-inhibited cells (Figure 3E, F). Consistent with recent data [17], in the absence of BRCA2, PrimPol recruitment at parental ssDNA in response to HU was barely affected by MRE11 inhibition (Figure 3F).

In the absence of BRCA2, the degraded reversed forks are subsequently converted into DSBs by MUS81/EME2 [36]. In contrast, loss or inhibition of RAD52 leads to fork degradation but without the induction of DNA breaks as the formation of MUS81-dependent DSBs also involves RAD52 [15,37]. Thus, we aimed to recapitulate the increased recruitment of Polα observed in the absence of RAD52 blocking MUS81-dependent DSBs in BRCA2-deficient cells (scheme in Figure 3G). To test this hypothesis, we analysed the association of POLA1 with parental ssDNA by performing PLA in doxycycline-inducible shBRCA2 cells knocked-out for MUS81 by CRISPR-Cas9 [38] (Figure 3G). As expected, downregulation of BRCA2 (Supplementary Figure 11) did not affect the number of POLA1-ssDNA PLA spots in MUS81 wild-type cells (Figure 3G). However, upon downregulation of BRCA2 in MUS81 KO cells, an increased formation of POLA1-ssDNA PLA spots was clearly detected (Figure 3G). In contrast, MUS81 knock-out did not stimulate POLA1-ssDNA association in BRCA2-proficient cells (see Doxy -; Figure 3G).

Altogether, these results indicate that, in response to replication fork arrest, POLA1 is *de novo* recruited downstream fork reversal as a consequence of fork degradation.

The function of Polα at perturbed replication forks involves interaction with RAD51.

We observe that recruitment of Polα in response to perturbed replication is origin-independent and depends on fork remodelling. In Xenopus extracts, Polα associates with Rad51 after replication arrest [39]. Thus, we tested if origin-independent recruitment of Polα that occurs following inhibition of RAD52 might involve association with RAD51. To this end, we first assessed the interaction between Polα and RAD51 by PLA after treatment with HU at different concentrations and times. Replication fork arrest resulted in the association of Polα with RAD51 already in cells in which RAD52 was not inhibited (U2OS WT), and this association increased with time becoming more evident at 4h of HU (Figure 4A). Interaction between Polα and RAD51 was higher and statistically significant in cells treated with the RAD52i, at both 2 and 4h of HU (Figure 4A). Similar to replication fork arrest, also replication fork perturbation by a low dose of HU resulted in enhanced interaction between Polα and RAD51 upon inhibition of RAD52 (Figure 4B). To further confirm that RAD52 inhibition stimulated Polα recruitment and association with RAD51 at

perturbed replication forks we performed correlative single-molecule localisation microscopy by dSTORM. Active replication forks were labelled with a short EdU pulse before challenging replication with 0.5mM HU in the presence or not of RAD52i (Figure 4C). After filtering out single labelling sites, co-localisation at the nanometry-scale was then assessed in tri-colour dSTORM through the analysis of the variation of signal clustering involving EdU-Polα or Polα-RAD51 at EdU+ sites (Figure 4D). These analyses confirmed the increase in the fraction of Polα at EdU+ sites observed with PLA and revealed that RAD52 inhibition resulted in a shift of the fraction of RAD51 molecules that engage in single interaction with the fork to the benefit of the fraction involved in the association with Polα at the EdU+ sites (Figure 4D, E). Furthermore, topology inspection suggested that Polα is found almost always at the end of the EdU signal that is preceded by or embedded into the RAD51 signal in the clustered analysis.

We next investigated whether RAD51 was functionally required for the hyper-recruitment of Polα observed after RAD52 inhibition. To do this, we evaluated the association of Polα with parental ssDNA after treatment with HU, in the presence or absence of RAD52i, by performing a PLA when RAD51 function was inhibited using the B02 compound (RAD51i; [40]). As shown in Figure 5A, in RAD52-proficient cells (WT), RAD51 inhibition did not significantly change the level of association between Polα and ssDNA upon replication arrest. In contrast, RAD51 inhibition led to a striking reduction in the number of PLA spots representing the association of Polα with ssDNA when RAD52 was inhibited (Figure 5A). Notably, RAD51 inhibition returned the level of Polα-ssDNA interaction to that detected in wild-type cells. To confirm this striking RAD51 dependency observed in the HU-induced recruitment of Polα when RAD52 is inhibited, we performed Western blotting on chromatin fractions from cells treated with 2mM HU for 4h. Recapitulating what was observed by PLA, analysis of chromatin-associated proteins showed more POLA1 associated with DNA in cells treated with RAD52i and HU and confirmed that concomitant inhibition of RAD51 reduced this association (Figure 5B). In RAD52-inhibited cells, both the association of Polα with parental ssDNA and the exposure of parental ssDNA, a readout of gap accumulation (see Figure 2), were RAD51-dependent following treatment with 0.5mM HU (Supplementary Figure 12).

RAD51 plays a role in promoting remodelling and protecting the extruded strand during fork reversal [41,42]. In addition, RAD51 may be required to promote recombination from the ssDNA produced at the reversed fork. To distinguish between the different roles of RAD51, we decided to deplete it using different concentrations of the J11 siRNA. High

concentrations have been reported to interfere with RAD51's function before fork reversal, which requires fewer RAD51 molecules, while low concentrations are sufficient to interfere with its function after fork reversal (fork protection or strand-invasion), which requires more RAD51 molecules [14].

As shown in Figure 5C, transfection with 2pmol of J11 siRNA led to only minor changes in the amount of RAD51 while 20pmol of oligos reduced the protein level of more than 80% with respect to the mock-transfected control. In RAD52 mock-inhibited cells (WT), recruitment of Polα at parental ssDNA in response to replication fork arrest was not affected by transfection with either 2pmol or 20pmol of the J11 RAD51 siRNA (Figure 5D). However, when RAD52 was inhibited, transfection with 2pmol of RAD51 J11 siRNA was nonetheless sufficient for a significant reduction in the level of Polα-ssDNA binding (Figure 5D). Following RAD52 inhibition, the HU-stimulated association between Polα and the ssDNA was also reduced by 20pmol of RAD51 J11 siRNA (Figure 6D), and this is consistent with the observed dependency of this Polα recruitment from fork reversal (see Figure 3). To further substantiate our observations, we analysed if inhibition of RAD51 before or in the last 2h of the HU treatment differently affected the association of Polα and ssDNA (scheme in Figure 5E). In the absence of RAD52i, inhibition of RAD51, either before or during the last 2h of HU treatment, did not affect the recruitment of Polα as seen by PLA (Figure 5E). In sharp contrast, inhibition of RAD51 decreased the enhanced Polα-ssDNA association observed when RAD52 was inhibited, and even exposure of cells to the RAD51i in the last 2h of treatment was effective (Figure 5E).

These results indicate that the origin-independent Polα recruitment and parental ssDNA accumulation stimulated by loss of RAD52 function during replication perturbation are dependent on the function of RAD51 upstream and downstream the reversed fork.

RAD51 nucleofilament formation directly stimulates Polα-primase function

Our data indicate that RAD52 inhibition promotes RAD51-mediated Polα recruitment following replication perturbation, leading to the formation of daughter-strand gaps. Given that RAD51 and Polα interact within the cell (Figure 5), we investigated whether RAD51 stimulates Polα-mediated repriming by testing its primase-polymerase activities through in vitro assays. To this end, we conducted a primer extension experiment using a 70nt-long model poly-dT template and recombinant Polα-Primase complex, with and without increasing amounts of RAD51. Reaction conditions were optimized to assess only the primase reaction while suppressing DNA synthesis (Supplementary Figure 13a-c). The

purified Polα/Primase complex successfully performed priming, resulting in the expected size of primed DNA (Figure 6a). Adding RAD51 to the reaction surprisingly increased the efficiency of the primase function, extending up to the full length of the template and, at higher concentrations of RAD51, even beyond (Figure 6a, b, and c), suggesting the joining of multiple templates by RAD51 nucleofilaments. RAD51 is a single-strand DNA binding protein. Thus, to determine if the observed stimulation of priming activity of Polα/Primase by RAD51 could be dependent on its ssDNA binding activity, we repeated the primer extension assay with purified RPA. As shown in Figure 6d-f, RPA completely suppressed the primase activity. We next decided to assess the effect of RAD51 using a more complex template DNA and selected the φX174 virion ssDNA, which is more than 5kb-long and circular. Consistently with the short poly-dT template, inclusion of RAD51 at increasing concentration in the primase reaction with Polα/Primase led to a great stimulation of primase activity and formation of extra-long products of priming (Figure 6g-i). Also in this case, RPA in the reaction resulted in suppression of even the expected Polα/Primase priming activity (Figure 6j-l). The stimulation by RAD51 was apparently limited to primase activity since switching into DNA synthesis-permissive conditions failed to show any stimulation of Polα-dependent DNA synthesis, which was rather decreased by the presence of RAD51 or RPA (Figure 6m-n). Since our biochemical data exclude that stimulation of Polα/Primase derives from the trivial recognition and wrapping of the ssDNA template, we decided to test if correct formation of RAD51 nucleofilaments was required for the observed boost in Polα/Primase activity. To this end, we selected to RAD51 mutants known to form unstable filaments (RAD51-T131P) or to be unable to assembly nucleofilaments (RAD51-F86E) [43,44]. As shown in Supplementary Figure 14a and b, both the RAD51 mutants abrogated, partially or completely depending on the level of impaired nucleofilament formation on template ssDNA (Supplementary Figure 14c).
Collectively, these results unveil an unexpected ability of RAD51 nucleofilaments to stimulate the priming by Polα/Primase leading to extra-long RNA primer formation.

Polα recruitment occurs downstream extended degradation at perturbed replication forks.

Our data suggest that, in the absence of a functional RAD52, MRE11-dependent degradation of nascent strand might contribute to Polα recruitment with a kinetics that might implicate extensive nucleolytic degradation and reset of the reversed fork. To test this hypothesis, we performed EdU pulse and chase SIRF experiments to define if

association of Polα with nascent DNA would have been detectable well behind the fork. We pulse-labelled active replication forks with EdU followed by chase in EdU-free medium and treatment with 0.5mM HU, to slow-down replication, in the presence or not of MIRIN and RAD52i (Figure 7A). Assuming 1/10th of normal replication fork rate in 0.5mM HU (~ 0.1 vs. 1Kb/min; [45]), these pulse and chase experiments were expected to locate labelled nascent DNA at different positions with respect to the delayed fork: close to it or far to it (Figure 7A). At the 5min chase time-point, SIRF assay confirmed the parental ssDNA PLA and dSTORM data showing an increased Polα proximity with EdU in RAD52i-treated cells (Figure 7B). Surprisingly, but consistent with the minimal effect of MRE11 inhibition on parental ssDNA (Figure 1), this recruitment was not affected by MIRIN. However, Polα proximity with EdU-labelled DNA was still clearly dependent on RAD51 (Figure 7B). At the 15min chase time-point, more Polα became associated with EdU-labelled DNA in RAD52 inhibited cells, however, this increased association was completely suppressed by MIRIN or RAD51i, which set the PLA signals back to the wild-type values (Figure 7C).

These results suggest that defective metabolism of stalled forks in RAD52 inhibited cells promotes two types of RAD51-dependent recruitment: one independent on fork degradation by MRE11 and another one dependent on extensive fork degradation, revealing the region of DNA labelled with EdU near which Polα could be loaded.

This second wave of Polα recruitment at EdU-labelled DNA together with dependency on fork reversal and MRE11 might implicate strand invasion from the gap formed at the reset reversed fork. While it is still uncertain if BRCA2 is involved in the pro-reversal function of RAD51 at the forks, its presence is important for the strand invasion activity or for recruitment of polymerases. Thus, we questioned if inhibition of RAD52 might stimulate association of RAD51 with EdU-labelled nascent DNA exposed at the perturbed replication fork and if this was BRCA2-dependent. To this end, we performed the SIRF experiment to localise RAD51 with EdU-labelled DNA in doxycycline-inducible shBRCA2 MRC5SV40 cells, using the 15min pulse-chase experiment described in Figure 7A. Under this scheme, we expect to observe a pool of RAD51 that is sensitive to BRCA2-depletion and that is engaged from the degraded forks and, possibly, another pool that is not affected by loss of BRCA2 since is loaded at the fork to promote its reversal. Treatment with 0.5mM HU in RAD52 mock-inhibited cells resulted in a variable number of EdU-RAD51 PLA spots, which was greatly increased upon RAD52 inhibition (Figure 7D). Doxycycline-driven BRCA2-depletion did not significantly reduce the number of RAD51 SIRF signals in wild-type cells, possibly because they preferentially represent recruitment of RAD51 before fork

reversal (Figure 7D). In contrast, the increased EdU-RAD51 PLA spots associated to RAD52 inhibition was largely reduced by depletion of BRCA2 (Figure 7D). Of note, and surprisingly, preventing fork breakage by MUS81 in the absence of BRCA2 resulted in an elevated number of RAD51 fork localisation, which was apparently all RAD52-dependent (Figure 7D), suggesting that RAD52 can substitute for BRCA2 under specific circumstance as previously reported in human cells [46,47]

In the absence of a functional RAD52, a pool of RAD51 and Polα is recruited also independently on MRE11-dependent fork degradation (see Figure 3C and 6B). Since Polα is recruited at the lagging strand, we asked if RAD52 might act on lagging strand gaps originating at perturbed replication forks. Thus, we tested if the presence of unreplicated parental ssDNA might stimulate RAD52 recruitment. To this end, we pre-treated cells with the POLA1i to block replication of the lagging strand [48]. Under this condition, and in the absence of any other treatment, we assumed that lagging strand gaps would be formed. Then, we evaluated association of RAD52 to parental ssDNA by PLA. Interestingly, pre-treatment with POLA1i substantially increased the association of RAD52 to parental ssDNA, mimicking what observed very early after HU treatment (Figure 7E).

Collectively, these results indicate that loss of RAD52 stimulates two different types of RAD51-dependent Polα recruitment in response to replication perturbation. One early and independent on fork degradation and a second late and dependent on fork degradation. Our data also suggest that RAD52 is recruited at lagging strand discontinuities.

RAD51-Polα-dependent repriming is involved in limiting the accumulation of DNA damage in RAD52-deficient cells.

Loss of RAD52 leads to a partial defect in fork restart after replication inhibition, mild genome instability and persistence of unreplicated regions in the subsequent cell cycle [15]. Having demonstrated that inhibition of RAD52 during replication fork perturbation stimulates a peculiar, origin-independent but RAD51-dependent, engagement of Polα, we asked if this mechanism might be protective against DNA damage and genome instability accumulation.

To this aim, we evaluated the accumulation of DNA damage by the analysis of γH2AX immunostaining after replication perturbation in mock (WT) or RAD52-inhibited U2OS cells. To interfere with the Polα-mediated repriming events, we exposed cells to the low dose of POLA1i during treatment (see Figures 2E, F and S8). As shown in Figure 8A, neither RAD52i or POLA1i alone significantly increased the yield of γH2AX-positive cells in

response to 0.5mM HU. However, combined with the RAD52i, treatment with POLA1i greatly enhanced the number of γH2AX-positive cells and the intensity of the staining.

Next, we evaluated if engagement of Polα-mediated repriming might counteract accumulation of chromosomal damage in cells inhibited of RAD52 and treated with HU by analysing GIEMSA-stained metaphase spreads. As expected, inhibition of RAD52 induced a mild increase in total chromosomal damage (Figure 8B, C). Treatment with POLA1i alone, did not induce any noticeable increase in wild-type cells while stimulated the total chromosomal damage if combined with RAD52 inhibition (Figure 8B, C). Most strikingly, combined inhibition of Polα and RAD52 did not increase the number of chromosomal breaks but greatly stimulated the number of chromosomal fusions and exchanges (Figure 8C, D). Thus, inhibition of the Polα-dependent pathway is sufficient to promote specifically the formation of complex chromosomal damage in the absence of a functional RAD52. Persistence of chromosomal damage or mitotic defects can be passed to the next generation and be visible as “scars” in terms of high 53BP1 nuclear bodies (53BP1 NBs). Thus, we evaluated the presence of 53BP1 NBs in U2OS cells recovering from perturbed replication after RAD52 inhibition or combined POLA1i and RAD52i treatment. As shown in Figure 8E, replication perturbation in the presence of the RAD52i led to some increase in the number of 53BP1 NBs as compared with non-inhibited cells. Most notably, combined treatment with RAD52i and POLA1i, significantly increased the fraction of cells with the higher number of 53BP1 NBs (Figure 8E).

Collectively, these results indicate that the RAD51-Polα pathway is a salvage mechanism that protect cells experiencing perturbed replication in the presence of a non-functional RAD52 from the accumulation of chromosomal damage and the passage to daughter cells of a damaged genome.

DISCUSSION

Here, we show that disabling the function of RAD52 is sufficient to induce accumulation of parental ssDNA gaps in response to perturbed replication. DNA gaps have been shown to frequently accumulate in cells exposed to replication stress and they can derive from either exonuclease-dependent targeting of the stalled forks, defective Okazaki fragment metabolism or from repriming events [3,49]. In human cells, repriming seems prevalently associated with the activity of PrimPol, a specialised polymerase-primase that has been shown to be activated after different kinds of replication perturbations [16,17,19,22,32,50].

Interestingly, our findings indicate that human cells can activate also PrimPol-independent repriming under certain circumstances. Indeed, loss or inhibition of RAD52-ssDNA association stimulates formation of gaps in the parental strand that are dependent on the activity of Polα, thus phenocopying what has been repeatedly reported in yeast [20,51]. This Polα-mediated formation of parental gaps is matched by a great increase in an origin-independent recruitment of Polα at parental ssDNA that supports the repriming activity rather than normal involvement in de-novo origin firing. Replication perturbation-dependent recruitment of Polα in the absence of RAD52, involves AND-1, whose recruitment is also stimulated. Since AND-1 normally assists loading and retention of Polα during lagging strand synthesis [33,52–54], it is likely that loss of RAD52 triggers a peculiar repriming activity at lagging strand as opposed to a specific or highly biased use of PrimPol that occurs at the leading strand [21]. Of note, some PrimPol recruitment still occurs in the absence of RAD52 but it is not stimulated upon replication arrest significantly, as observed in RAD52-proficient cells and much more in BRCA2-depleted cells.

Our data indicate that, in RAD52-deficient cells, the Polα recruitment and Polα-stimulated accumulation of parental ssDNA occur downstream fork reversal as they are strongly reduced by downregulation of SMARCAL1, the critical enzymes involved in fork remodelling [9]. This is paralleled by a dependency on MRE11 activity suggesting that most if not all of the Polα-mediated repriming occurring in RAD52-deficient cells is a response to extensive fork degradation, which happens when RAD52 is inhibited [15]. These findings differentiate such Polα-mediated repriming from that mediated by PrimPol, which acts in parallel with the fork reversal [16]. However, why loss of RAD52 or BRCA2 stimulates fork degradation but does not stimulate the same repriming pathway? In BRCA2-deficient cells, degradation of the reversed fork is followed by endonucleolytic cleavage by MUS81/EME2 and break-induced replication to promote restart of DNA synthesis [36]. Loss of RAD52

promotes fork degradation but does not induce fork cleavage because RAD52 also regulates MUS81-dependent DSBs [37]. Depletion of MUS81 in BRCA2-deficient cells leads to extended fork degradation, which is the same observed in cells inhibited of RAD52 during replication arrest [15]. Most importantly, preventing MUS81 from cleaving at the degraded reversed fork in BRCA2-deficient cells is sufficient to stimulate the recruitment of Polα at parental ssDNA (Figure 3G). This suggest that extended degradation, which might reset the reversed fork, could also promote repriming on both DNA strands as shown in yeast [20]. Interestingly, in response to 2mM HU, a dose that completely blocks replication, we detect increased recruitment of Polα during treatment. However, we only detect parental ssDNA accumulation during recovery from HU. This supports the hypothesis that increased exposure of parental ssDNA derives from the peculiar repriming activity combined with extensive nascent strand degradation, which probably takes place when replication is resumed or only delayed when cells are treated with the low-dose of HU.

We find that Polα-dependent ssDNA gaps and Polα recruitment under perturbed replication are dependent on RAD51 especially in the absence of RAD52. Moreover, our data show that Polα and RAD51 interacts under these conditions. RAD51 is important for fork restart and has been previously shown to interact with Polα for its localisation at the fork [39]. Furthermore, it has been reported that RAD51 and MRE11 can stimulate an origin-independent re-loading of the replisome at collapsed replication forks [55]. However, our data indicate that RAD51-dependent Polα recruitment occurs independently of fork collapse and downstream fork reversal/degradation. This differentiates this recruitment from that reported previously, which has been shown to happen before fork reversal to limit its excessive engagement or to assist replication of lagging strand [39,56]. Our findings also show that even a small reduction in the amount of RAD51 is sufficient to interfere with Polα recruitment and gap accumulation. It has been reported that only the extensive RAD51 nucleation associated to fork protection or strand invasion is sensitive to limited depletion [14]. As inhibition of RAD52 *per se* induces fork deprotection in wild-type cells [15], our results might suggest that Polα is recruited downstream a strand-invasion event post fork reversal. Consistent with this, inhibition of RAD52 leads to an increased and BRCA2-dependent recruitment of RAD51 at the nascent DNA left behind the perturbed forks. These observations would be consistent with the engagement of recombination-dependent replication (RDR) started from the uncut 3'-flap generated by the extensive degradation of the reversed fork. This mechanism has been well characterized in yeast but only few data were available in human cells [42,57–59]. Furthermore, in yeast, DNA synthesis during RDR is

dependent on Polδ but minimally involves Polα [60]. Instead, our data suggest that Polα is essential for RDR in human cells, at least when RAD52 is inactivated. Interestingly, our biochemical experiments confirm that RAD51 nucleofilaments formed onto ssDNA templates can specifically stimulate Polα-mediated priming and evidence how primer extension is pushed well beyond the usual limit known to exist during normal replication. Further investigations would be required to characterize these points. In yeast, mutations leading to extensive processing of reversed forks can stimulate either Polα repriming or template-switching and repriming post strand invasion, which might be dependent on Polα/primase [20,61]. Thus, our observations could support a similar mechanism also in human cells, demonstrating that PrimPol is not the only available repriming mechanism. Of note, we find that RAD52 recruitment is stimulated by a treatment inducing a biased discontinuity in the lagging strand to the same extent observed when cells are challenged with a low-dose of HU. This result might be consistent with the observed role of RAD52 at the fork in preventing unscheduled activity of SMARCAL1 [15]. Indeed, SMARCAL1 recruitment should be restrained to the leading strand to establish productive intermediates for subsequent replication restart [62]. The strong recruitment of RAD52 at parental ssDNA induced by formation of lagging strand gaps would be consistent with the AND-1-dependent recruitment of Polα, which is expected to take place at lagging strand. Interestingly, it has been recently reported that also Polθ can be recruited at the lagging strand to fill-in template gaps in the absence of RAD51 [56,63]. Thus, multiple mechanism might contribute to prevent excessive fork reversal and accumulation of template gaps in the lagging strand.

We previously demonstrated that inhibition of RAD52, although determining a striking fork degradation phenotype, does not impair as strongly fork restart [15]. This was not unexpected since fork degradation is not associated to a significant decrease in fork restart also in BRCA2-deficient cells [64]. However, in BRCA2-deficient cells, restart has been proposed to occur through at least two pathways: BIR and repriming by PrimPol [31,36]. Inhibition of Polα limits fork restart in the absence of RAD52, indicating that when forks get degraded, but BIR cannot be engaged, cells have another additional mechanism to channel extensively degraded forks into a “secondary” recombination-dependent restart pathway. This “secondary” pathway is however important to limit DNA damage in response to perturbed replication. Indeed, the mild inhibition of Polα not only reduces fork restart but strikingly increases signs of replication stress, such as γH2AX foci and chromosomal

damage. This backup pathway might also contribute to explain why RAD52 knock-down in humans does not generate a strong phenotype [11].

Altogether, our findings may be summarized in the model proposed in Figure 8F. Replication perturbation, by uncoupling unwinding from DNA synthesis, stimulates the recruitment of RAD52 at the fork, among others. Recruitment of RAD52, most probably at a lagging strand discontinuities, acts as a gatekeeper limiting unscheduled and perhaps "error-prone" engagement of SMARCAL1, as previously demonstrated [15]. When fork protection is defective but the MUS81 complex can cleave the presumably long 3'-flap formed downstream MRE11-EXO1, the perturbed fork can be restarted using BIR. When the degraded reversed fork cannot be cleaved by MUS81, as in the absence of RAD52, on one hand, BRCA2 and RAD51 promotes Polα recruitment at the lagging strand gap, with or without intervention of an unknown exonuclease. On the other hand, RAD51-dependent Polα recruitment might take place at the extruded nascent lagging strand of the reversed fork DNA after degradation of the complementary strand, promoting template-switch and resulting in template gaps after branch migration of the D-loop. Currently, we cannot give clues on to what extent the two RAD51-dependent recruitment of Polα are interlinked. Similarly, we cannot exclude that RAD51 assists Polα-mediated repriming in the lagging strand, which is not involved in RDR. In both cases, this mechanism would support fork restart and limit DNA damage that otherwise accumulates upon replication perturbation in the absence of RAD52 (Figure 8). Alternatively, BRCA2 and RAD51-dependent Polα recruitment might occur after the reset of the fork downstream template-switch from a leading or, most likely, a lagging strand gap.

RAD52 can be found mutated in cancer [65]. It will be interesting to assess if cancer-related mutations disable the gatekeeper role of RAD52 predisposing cells to use Polα-mediated repriming and becoming hypersensitive to inhibitors of Polα. Moreover, RAD52 loss or inhibition is extremely synthetic sick with loss of BRCA2 or the checkpoint [37,66,67]. The interaction between RAD51 and Polα has been preliminary mapped in the Xenopus model system [39], and separation of function would be a useful tool to further characterize this mechanism and determine if this genetic relationship also correlates with an inability to perform RAD51-Polα-mediated repriming at distressed forks.

MATERIALS AND METHODS

Cell lines and culture conditions

The MRC5SV40 and human osteosarcoma cell line (U2OS) were maintained in Dulbecco's modified Eagle's medium (DMEM, Euroclone) supplemented with 10% fetal bovine serum (Euroclone) and incubated at 37 °C in a humidified 5% CO2 atmosphere. MRC5SV40 shRAD52 were obtained by transfection with a lentivirus expressing two different shRNA sequences (SigmaAldrich Mission lentivirus, sequence codes 271352 (V2)). MRC5SV40 KO PrimPol cells were a kind gift from Professor Aidan Doherty of Sussex University. MRC5SV40 KO MUS81 cells were obtained with the Crispr/Cas9 system by using two Alt-R® Crispr-Cas9 gRNA (Hs.Cas9.MUS81.1.AA and Hs.Cas9.MUS81.1.AB) and successively transfected with the WT protein [38]. MRC5SV40 shBRCA2 or U2OS shSMARCAL1 were transfected with lentiviruses expressing the shSMARCAL1 or shBRCA2 cassette under the control of a doxycycline (Dox)-regulated promoter, at 0.5 of multiplicity of infection (MOI) (Dharmacon SmartVector inducible lentivirus, sequence code: V3SH11252-227970177 (shSMARCAL) and V3SH7669-226099147 (shBRCA2). After puromycin selection at 300 ng/ml, a single clone was selected and used throughout the study. SMARCAL1 overexpressing U2OS were obtained by the transfection of U2OS WT cells with the inducible PiggyBac/Transposase system, in a proportion of 9:1 [35]. Cell lines were routinely tested for mycoplasma contamination and maintained in cultures for no more than one month.

Oligos and plasmids

siRNA

WDHD1 (AND-1)	Sigma Aldrich MISSION esiRNA #EHU134421
ZRANB3	Dharmacon siGENOME siRNA D-010025-03-005 cat # 84083
MUS81	Qiagen FlexiTube siRNA cat # SI04300877 oligo #6
BRCA2	Dharmacon ON TARGET PLUS SMARTpool siRNA #SO-2994934G
RAD51 (J11)	Dharmacon ON TARGET PLUS siRNA #SO-2960294G

Plasmids

peGFP-PrimPol WT	Bailey et al., 2019
PiggyBac-SMARCAL1	Pugliese et al., 2019

WT	
pFLAG-MUS81 WT	Palma et al., 2018

Transfections

All the siRNAs were transfected using Interferin® (Polyplus) 48 h before to perform experiments. WDHD1 siRNA was used at 10 nM. RAD51 siRNA (J11) was used at 2 and 20 pmol. MUS81 and BRCA2 siRNAs were used at 25 nM. ZRANB3 siRNA was used at 50 nM. The peGFP-PrimPol, PiggyBac-SMARCAL1 and pFLAG-MUS81 were transfected in cell lines using NeonTM transfection system (Invitrogen) 48 h prior to perform experiments.

Chemicals

HU (Sigma-Aldrich) was added to culture medium at 2 mM or 0.5 mM from a 200 mM stock solution prepared in Phosphate-buffer saline solution (PBS 1X) to induce DNA replication arrest or slowing. RAD52 inhibitor, Epigallocatechin (EGC - Sigma-Aldrich) was dissolved in DMSO at 100 mM and used at 50 µM. The B02 compound (Selleck), an inhibitor of RAD51 activity, was used at 27 µM. CDC7i (XL413, Selleck) was dissolved in sterile water and used 10 µM. Doxycycline (Sigma-Aldrich) was dissolved in DMSO and used 1µ/ml. MIRIN, the inhibitor of MRE11 exonuclease activity (Calbiochem), was used at 50 µM. Polα inhibitor (ST1926 – Sigma-Aldrich) was dissolved in DMSO and used at the concentrations reported on the experiments. S1 nuclease (Invitrogen cat # 18001016) was diluted 1/100 in S1 buffer and used at 20 U/ml. CldU (Sigma-Aldrich) was dissolved in sterile water as a 200 mM stock solution and used at 50 µM. IdU (Sigma-Aldrich) was dissolved in sterile DMEM as a stock solution 2.5 mM and used at 100 for ssDNA and PLA assays or 250 µM for fibers assay. 5-ethynyl-2'-deoxyuridine (EdU) (Sigma-Aldrich) Was dissolved in DMSO and used at 10 µM for EdU incorporation assay or 100 µM for SIRF assay.

Western blot analysis

Western blots were performed using standard methods. Blots were incubated with primary antibodies against: anti-GFP (Santa Cruz Biotechnology, 1:500), anti-MUS81 (Santa Cruz Biotechnology, 1:1000), anti-LAMIN B1 (Abcam, 1:10,000), anti-GAPDH (Millipore, 1:5000), anti-RAD51 (Abcam 1:10,000), anti-SMARCAL1 (Bethyl 1:1500), anti-ZRANB3 (Proteintech 1:1000), anti-BRCA2 (Bethyl 1:5000), anti-POLA1 (Polα - Bethyl, 1:500), anti-

WDHD1 (Novus Biologicals, 1:1000). After incubations with horseradish peroxidase-linked secondary antibodies (Jackson ImmunoResearch, 1:20,000), the blots were developed using the chemiluminescence detection kit ECL-Plus (Amersham) according to the manufacturer's instructions. Quantification was performed on blot acquired by ChemiDoc XRS+ (Bio-Rad) using Image Lab software, the normalization of the protein content was done through LAMIN B1 or GAPDH immunoblotting.

Chromatin isolation

After the treatments, cells (4 × 106 cells/ml) were resuspended in buffer A (10 mM HEPES, [pH 7.9], 10 mM KCl, 1.5 mM MgCl2, 0.34 M sucrose, 10% glycerol, 1 mM DTT, 50 mM sodium fluoride, protease inhibitors [Roche]). Then was added Triton X-100 at a final concentration of 0.1% and the cells were incubated for 5 min on ice. Nuclei were collected in pellet by low-speed centrifugation (4 min, 1300 × g, 4 °C) and washed once in buffer A. Nuclei were then lysed in buffer B (3 mM EDTA, 0.2 mM EGTA, 1 mM DTT, protease inhibitors) for 10 min on ice. Insoluble chromatin was collected by centrifugation (4 min, 1700 × g, 4 °C), washed once in buffer B + 50 mM NaCl, and centrifuged again under the same conditions. The final chromatin pellet was resuspended in 2X Laemmli buffer and sonicated for 15 s in a Tekmar CV26 sonicator using a microtip at 50% amplitude.

EdU incorporation assay

U2OS were treated with 10 μM EdU 10 min before giving the treatment with ST1926 for 30 min at the indicated concentrations. After the treatment, cells were permeabilized with 0.5% TritonX-100 in PBS 1X for 10 minutes on ice, then fixed with 3% PFA, 2% sucrose in PBS 1X at room temperature (RT) for 15 min. For the EdU detection was applied the Click-iT™ EdU Alexa Fluor™ 488 Imaging Kit (Invitrogen) for 30 minutes at RT. The reagents for the Click-iT™ reaction were diluted according to the manufacturer's instructions. Nuclei were examined with Eclipse 80i Nikon Fluorescence Microscope, equipped with a Virtual Confocal (ViCo) system and foci were scored at 40X magnification. Quantification was carried out using the ImageJ software.

IdU incorporation assay

MRC5SV40 and U2OS were treated with 100 μM IdU for 20 hours and released for 2 hours in fresh DMEM before giving the treatment with RAD52i and HU for 4 hours at the reported concentrations. After the treatment, cells were fixed at RT with 4% PFA/PBS for

10 min, permeabilized with 0.4% TritonX-100/PBS and denatured with 2.5 N HCl/PBS for 45 minutes. Cells were then incubated with mouse anti-IdU antibody (Becton Dickinson, 1:80) for 1 h at 37 °C in 1% BSA/PBS, followed by species-specific fluorescein-conjugated secondary antibodies (Alexa Fluor 488 Goat Anti-Mouse IgG (H + L), highly cross-adsorbed—Life Technologies). Slides were analysed with Eclipse 80i Nikon Fluorescence Microscope, equipped with a Virtual Confocal (ViCo) system. Quantification was carried out using the ImageJ software.

Detection of ssDNA by native IdU assay

To detect parental ssDNA, cells were labelled for 20 hours with 50 μM IdU (Sigma-Aldrich), released in fresh DMEM for 2 hours, then treated as indicated. For immunofluorescence, cells were washed with PBS 1X, permeabilized with 0.5% Triton X-100 for 10 min at 4 °C and fixed in 3% PFA, 2% sucrose in PBS 1X. Fixed cells were then incubated with mouse anti-IdU antibody (Becton Dickinson, 1:80) for 1 h at 37 °C in 1% BSA/PBS, followed by species-specific fluorescein-conjugated secondary antibodies (Alexa Fluor 488 Goat Anti-Mouse IgG (H + L), highly cross-adsorbed—Life Technologies). Slides were analysed with Eclipse 80i Nikon Fluorescence Microscope, equipped with a Virtual Confocal (ViCo) system. For each time point, at least 100 nuclei were analysed. Quantification was carried out using the ImageJ software.

In situ PLA assay for ssDNA–protein interaction

The in-situ PLA NaveniFlex (Navinci Diagnostics) was performed according to the manufacturer's instructions. For parental ssDNA-protein interaction, cells were labelled with 100 μM IdU for 20 hours and then released in fresh medium for 2 hours. After treatment, cells were permeabilized with 0.5% Triton X-100 for 10 min at 4 °C, fixed with 3% PFA/2% sucrose in PBS 1X for 10 min and then blocked in 3% BSA/PBS for 15 min. After washing with PBS, cells were incubated with the two relevant primary antibodies. The primary antibodies used were as follows: mouse monoclonal anti-RAD51 (GeneTex, 1:150), mouse monoclonal anti-IdU (Becton Dickinson, 1:50), rabbit polyclonal anti-Polα (Bioss, 1:50), rabbit polyclonal anti-GFP (Invitrogen 1:150), rabbit anti-WDHD1 (Novus Biologicals, 1:50), rabbit anti-RAD52 (Aviva, 1:150). The negative controls were obtained by using only one primary antibody. Samples were incubated with secondary antibodies conjugated with PLA probes MINUS and PLUS: the PLA probe anti-mouse PLUS and anti-rabbit MINUS (NaveniFlex equivalent). The incubation with all antibodies was

accomplished in a humidified chamber for 1 h at 37 °C. Next, the PLA probes MINUS and PLUS were ligated using two connecting oligonucleotides to produce a template for rolling-cycle amplification. After amplification, the products were hybridized with red fluorescence-labelled oligonucleotide. Samples were mounted in Prolong Gold anti-fade reagent with DAPI (blue). Images were acquired randomly using Eclipse 80i Nikon Fluorescence Microscope, equipped with a Virtual Confocal (ViCo) system. The analysis was carried out by counting the PLA spot for each nucleus. To exclude the cells outside the S-phase from the analysis, nuclei with less than 7 (treated) or 2 spots (untreated) were considered as negative.

Single-cell Assay for in situ Protein Interaction with Nascent DNA (SIRF)

Exponential growing cells were seeded onto microscope chamber slide. The day of experiment, cells were incubated with 100 µM EdU for 20 min and treated as indicated. After treatment, cells were pre-extracted in 0.5% TritonX-100 for 5 min on ice and fixed with 3% PFA, 2% sucrose in PBS 1X for 15 min at RT. Cells were then blocked in 3% BSA/PBS for 15 min. For the EdU detection was applied the Click-iT™ EdU Alexa Fluor™ Imaging Kit (Invitrogen) using 5mM Biotin-Azide for 30 minutes at RT. The primary antibodies used were as follows: mouse monoclonal anti-RAD51 (GeneTex, 1:150), rabbit polyclonal anti-Polα (Bioss, 1:50), mouse anti-biotin (Invitrogen, 1:50) rabbit anti-biotin (Abcam, 1:50). The negative controls were obtained by using only one primary antibody. Samples were incubated with secondary antibodies conjugated with PLA probes MINUS and PLUS: the PLA probe anti-mouse PLUS and anti-rabbit MINUS (Duolink®, Sigma-Aldrich). The incubation with all antibodies was accomplished in a humidified chamber for 1 h at 37 °C. Next, the PLA probes MINUS and PLUS were ligated using two connecting oligonucleotides to produce a template for rolling-cycle amplification. After amplification, the products were hybridized with red fluorescence-labelled oligonucleotide. Samples were mounted in Prolong Gold anti-fade reagent with DAPI (blue). Images were acquired randomly using Eclipse 80i Nikon Fluorescence Microscope, equipped with a Virtual Confocal (ViCo) system. The analysis was carried out by counting the SIRF spot for each nucleus.

Single-Molecule Localisation Microscopy

U2OS cells were treated as indicated in the experimental scheme. After the treatment, cells were fixed and immunofluorescence was performed as described by Whelan & Rothenberg, 2021. EdU was detected with the Click-iT™ EdU Alexa Fluor™ Imaging Kit (Invitrogen) for 30 minutes at RT. Coverslips with fixed cells were stored for up to 1 week at 4 °C prior to dSTORM imaging. The fixed cells on coverslips were mounted onto concave slides and dSTORM imaging B3 buffer from Oxford Nanoimaging (ONI, PN #900-00004) was added before imaging. A commercial TIRF microscope (Nanoimager S Mark IIB from ONI, https://oni.bio) with lasers of 405 nm/150 mW, 488 nm/1 W, 561 nm/1 W, and 640 nm/1 W was used to acquire data. Briefly, fluorophore emission was collected by an oil immersion 100x/1.45NA objective and images were acquired at 30 ms exposure time using a Hamamatsu ORCA-Flash4.0 V3 Digital sCMOS camera. The reconstruction of the super-resolution image was conducted by NimOS software from ONI. Localization data were then analyzed using the ONI-CODI platform for drift correction, filtering, clustering, and counting.

Protein Preparation

Homogeneity human protein sample preparation of Polα/primase [68], RPA [69] and RAD51 [70] have been described. Site-specific F86E and T131P mutations were introduced in the RAD51 genes in the plasmids by Genscript mutagenesis service (Genscript, Piscataway, NJ) and corresponding RAD51 mutant protein were prepared as wild type.

Primase Assay

The priming activity of human Polα/primase was tested on poly-dT_{70} (IDT, Coralville, IA). Indicated amount of Polα/primase and ssDNA templates (500 nM) were incubated at 30 °C for 60 min in a standard reaction (20 µl) consisted of 20 mM Tris-Acetate (pH 8.0), 50 mM NaCl, 50 mM NaCl, 4 mM $MgCl_2$, 1 mM spermidine, 5 mM DTT, 0.5 µM [α-^{32}P] ATP (3000 Ci/mmol^{-1} , Revvity) , 50 µM unlabelled ATP and 4 U of RiboLock RNase Inhibitor (Thermo Scientific). The indicated amount of RAD51 or RPA was added into the reaction and held for 5 min before adding Polα/primase. Reaction products were mixed with 30 µl formamide loading buffer (90% formamide, 30 mM EDTA, 0.5× TBE, 0.1% of bromophenol and 0.025% SDS) and heated at 80 °C for 5 min. Samples (10 µl) were loaded on a sequencing-style 15% acrylamide, 7 M urea, 1× TBE gel. The bromophenol blue dye was run to the bottom of the gel (90 min, 250V). Radiolabeled RNA synthesis products were imaged on a FLA-7000 image scanner (FUJIFILM). Unless indicated otherwise, Polα–

primase activity was determined by total counts per spot or relative product (%) in which 100% indicate total counts of Polα/Primase only products.

Primer Extension Assay

RNA primer extension activities of the Polα/primase in various conditions were compared in reactions (20 µl) that contained the 0.5 µM poly-dT_{70} template with Cy3 fluorophore-labeled poly-rA_{15} RNA oligos. The annealing of the template with RNA primers was done by a decrease of temperature from 90 to 25 °C in 0.2 °C/min gradient in the thermo cycler. Reactions were assembled on ice in the following order. The primer/template was added to the buffer containing 20 mM Tris-HCl (pH 7.5), 50 mM NaCl, 10 mM $MgCl_2$, 0.2 mg/ml BSA, and 2 mM DTT followed by the addition of dATP (0.2 mM). Then, the indicated amount of RAD51 or RPA was added into the reaction and held for 5 min before Polα/primase was added and further incubated for 30 min at 30 °C. Reaction products were separated as described in primase assay. Visualization of the products used the Chemidoc MP imager (Bio-Rad).

Electrophoresis Mobility Shift Assay

Indicated concentrations of RAD51 or RPA were mixed with 500 nM of 5'-end Cy3 labeled poly-dT70 DNA substrates in a 15 µl of standard priming reaction buffer. The reaction mixtures were incubated at 30°C for 5 min then 1.5 µl of 10x Orange-G loading dye [0.1% Orange-G, 50% glycerol, 400 mM Tris-Acetate (pH 8.0) and 10 mM EDTA] was added. The bound and free DNA species were resolved by the non-denaturing 5.5% polyacrylamide gel electrophoresis in TAE buffer [40 mM Tris-Acetate (pH 8.0) and 1 mM EDTA]. The gel was imaged using a ChemiDoc MP (Bio-Rad) by exciting and monitoring Cy3 fluorescence.

DNA fibers analysis

Fiber's assay using S1 nuclease was performed as indicated by Quinet et al., 2017. Briefly, cells were pulse-labelled with 50 µM CldU and then labelled with 250 µM IdU with or without treatment, as reported in the experimental schemes. At end of treatment, cells were permeabilized with CSK buffer (100 mM NaCl, 10 mM PIPES pH 6.8, 1M EGTA, 3 mM MgCl2, 300 mM sucrose, 0.5% Triton X-100) for 10 min at RT, then were washed with PBS 1X and S1 nuclease buffer (30 mM sodium acetate, 10 mM zinc acetate, 5% glycerol, 50 mM NaCl) prior to add +/- S1 nuclease for 30 min at 37 °C in a humidified

chamber. Cells were washed with S1 buffer then scraped with 0.1% BSA/PBS and collected pellets were used to perform fibers spreading. For the fork progression assay, cells were pulse-labelled with 50 μM CldU for 20 min and then labelled with 250 μM IdU for 40 min, with or without RAD52i. DNA fibers were spread out as described [27]. For immunodetection of labelled tracks, the following primary antibodies were used: rat anti-CldU/BrdU (Abcam 1:50) and mouse anti-IdU/BrdU (Becton Dickinson 1:10). Images were acquired randomly from fields with untangled fibers using Eclipse 80i Nikon Fluorescence Microscope, equipped with a Virtual Confocal (ViCo) system. The length of labelled tracks was measured using the Image-Pro-Plus 6.0 software.

Chromosomal aberrations

MRC5SV40 cells were treated with HU 2 mM, with or without RAD52 inhibitor and/or Polα inhibitor, left at 37 °C for 4 hours, then allowed to recover in fresh medium for additional 24 hours. Cell cultures were incubated with colcemid (0.2 μg/ml) at 37 °C for 3 hours until harvesting. Cells for metaphase preparations were collected and prepared as previously reported [71]. For each condition, at least 50 chromosomes were examined, and chromosomal damage scored at 100× magnification.

Statistical analysis

Experiments shown are representative of at least two independent biological replicates unless otherwise indicated in the figure legend. Significance was assessed using the built-in tools in Prism 9 (GraphPad Inc.) by Kruskal-Wallis' test followed by post-hoc Dunn test for FDR for experiments with more than two samples, and by the two-tailed Student's t-test to evaluate the means from normal distributions when analysing two samples. $P < 0.05$ was considered as significant. Statistical significance was always denoted as follow: ns = not significant; *$P < 0.05$; **$P < 0.01$; ***$P < 0.01$; ***$P < 0.001$. If not otherwise indicated in the figure legend, analysis was performed by Kruskal-Wallis' test followed by post-hoc Dunn. Specific statistical analyses are reported in the relevant legend. No statistical methods or criteria were used to estimate sample size or to include/exclude samples.

ACKNOWLEDGMENTS

We thank Prof. Aidan Doherty for PrimPol KO cells and GFP-PrimPol expressing plasmid. We thank Dr. Patricia Kannouche for the MRC5SV40 cells. We want to thank Prof. Maria Spies and Luca Pellegrini for helpful discussion and advise. This work was supported by NIH-NCI grant (grant n. R01CA232425-A1) and by investigator grants from Associazione Italiana per la Ricerca sul Cancro (AIRC) to P.P. (IG n. 21428) and to A.F. (IG n. 19971).

AUTHORS CONTRIBUTION

L.D.B performed all experiments to analyse formation and mechanism of Polα-dependent parental DNA gaps using RAD52i. E.M. performed analysis of parental ssDNA formation in RAD52 knockdown cells and contributed to S1 DNA fiber assay. F.A.A. performed dSTORM experiments. P.V. performed the analyses of chromosome damage. All authors contributed to design experiments and analyze data. P.P and A.F. designed experiments, analysed data and supervised the project. L.D.B. contributed to write results. P.P. wrote the paper. All authors contributed to revise the paper.

CONFLICT OF INTEREST

The authors declare to do not have any conflict of interest

REFERENCES

1. Flynn, R. L. & Zou, L. ATR: A master conductor of cellular responses to DNA replication stress. *Trends Biochem. Sci.* **36**, 133–140 (2011).
2. Zeman, M. K. & Cimprich, K. A. Causes and consequences of replication stress. *Nat. Cell Biol.* **16**, 2–9 (2014).
3. Thakar, T. & Moldovan, G. The emerging determinants of replication fork stability. *Nucleic Acids Res.* **49**, 7224–7238 (2021).
4. Franchitto, A. & Pichierri, P. Replication fork recovery and regulation of common fragile sites stability. *Cell. Mol. Life Sci.* **71**, 4507–4517 (2014).
5. Pasero, P. & Vindigni, A. Nucleases Acting at Stalled Forks: How to Reboot the Replication Program with a Few Shortcuts. *Annu. Rev. Genet.* **51**, 477–499 (2017).
6. Berti, M., Cortez, D. & Lopes, M. The plasticity of DNA replication forks in response to clinically relevant genotoxic stress. *Nat. Rev. Mol. Cell Biol.* **21**, 633–651 (2020).
7. Neelsen, K. J. & Lopes, M. Replication fork reversal in eukaryotes: from dead end to dynamic response. *Nat. Rev. Mol. Cell Biol.* **16**, 207–20 (2015).
8. McGlynn, P. & Lloyd, R. G. Genome stability and the processing of damaged replication forks by RecG. *Trends Genet. TIG* **18**, 413–419 (2002).
9. Joseph, S. A. *et al.* Time for remodeling: SNF2-family DNA translocases in replication fork metabolism and human disease. *DNA Repair* **95**, 102943 (2020).
10. Kolinjivadi, A. M. *et al.* Moonlighting at replication forks - a new life for homologous recombination proteins BRCA1, BRCA2 and RAD51. *FEBS Lett.* 1–18 (2017) doi:10.1002/1873-3468.12556.
11. Malacaria, E., Honda, M., Franchitto, A., Spies, M. & Pichierri, P. Physiological and Pathological Roles of RAD52 at DNA Replication Forks. *Cancers* **12**, 402 (2020).
12. Leuzzi, G., Marabitti, V., Pichierri, P. & Franchitto, A. WRNIP1: A new guardian of genome integrity at stalled replication forks. *Mol. Cell. Oncol.* **3**, e1215777 (2016).

13. Couch, F. B. *et al.* ATR phosphorylates SMARCAL1 to prevent replication fork collapse. *Genes Dev.* **27**, 1610–1623 (2013).
14. Bhat, K. P. *et al.* RADX Modulates RAD51 Activity to Control Replication Fork Protection. *Cell Rep.* **24**, 538–545 (2018).
15. Malacaria, E. *et al.* Rad52 prevents excessive replication fork reversal and protects from nascent strand degradation. *Nat. Commun.* **10**, 1–19 (2019).
16. Quinet, A. *et al.* PRIMPOL-Mediated Adaptive Response Suppresses Replication Fork Reversal in BRCA-Deficient Cells. *Mol. Cell* **77**, 461-474.e9 (2020).
17. Tirman, S. *et al.* Temporally distinct post-replicative repair mechanisms fill PRIMPOL-dependent ssDNA gaps in human cells. *Mol. Cell* **81**, 4026-4040.e8 (2021).
18. Bai, G. *et al.* HLTF Promotes Fork Reversal, Limiting Replication Stress Resistance and Preventing Multiple Mechanisms of Unrestrained DNA Synthesis. *Mol. Cell* **78**, 1237-1251.e7 (2020).
19. Bianchi, J. *et al.* Primpol bypasses UV photoproducts during eukaryotic chromosomal DNA replication. *Mol. Cell* **52**, 566–573 (2013).
20. Fumasoni, M., Zwicky, K., Vanoli, F., Lopes, M. & Branzei, D. Error-Free DNA Damage Tolerance and Sister Chromatid Proximity during DNA Replication Rely on the Polα/Primase/Ctf4 Complex. *Mol. Cell* **57**, 812–823 (2015).
21. Guilliam, T. & Doherty, A. PrimPol—Prime Time to Reprime. *Genes* **8**, 20 (2017).
22. Piberger, A. L. *et al.* PrimPol-dependent single-stranded gap formation mediates homologous recombination at bulky DNA adducts. *Nat. Commun.* **11**, 1–14 (2020).
23. Branzei, D. & Szakal, B. DNA damage tolerance by recombination: Molecular pathways and DNA structures. *DNA Repair* **44**, 68–75 (2016).
24. Quinet, A., Tirman, S., Cybulla, E., Meroni, A. & Vindigni, A. To skip or not to skip: choosing repriming to tolerate DNA damage. *Mol. Cell* 1–10 (2021) doi:10.1016/j.molcel.2021.01.012.
25. Cortez, D. Replication-Coupled DNA Repair. *Mol. Cell* **74**, 866–876 (2019).

26. Hengel, S. R., Spies, M. A. & Spies, M. Small-Molecule Inhibitors Targeting DNA Repair and DNA Repair Deficiency in Research and Cancer Therapy. *Cell Chem. Biol.* **24**, 1101–1119 (2017).
27. Iannascoli, C., Palermo, V., Murfuni, I., Franchitto, A. & Pichierri, P. The WRN exonuclease domain protects nascent strands from pathological MRE11/EXO1-dependent degradation. *Nucleic Acids Res.* **43**, 9788–803 (2015).
28. Peng, M. *et al.* Opposing Roles of FANCJ and HLTF Protect Forks and Restrain Replication during Stress. *Cell Rep.* **24**, 3251–3261 (2018).
29. Quinet, A., Carvajal-Maldonado, D., Lemacon, D. & Vindigni, A. Chapter Three – DNA Fiber Analysis: Mind the Gap! in *Methods in Enzymology* vol. 591 55–82 (2017).
30. Cong, K. *et al.* Replication gaps are a key determinant of PARP inhibitor synthetic lethality with BRCA deficiency. *Mol. Cell* **81**, 3128-3144.e7 (2021).
31. Kang, Z. *et al.* BRCA2 associates with MCM10 to suppress PRIMPOL-mediated repriming and single-stranded gap formation after DNA damage. *Nat. Commun. 2021 121* **12**, 1–12 (2021).
32. Bailey, L. J., Bianchi, J. & Doherty, A. J. PrimPol is required for the maintenance of efficient nuclear and mitochondrial DNA replication in human cells. *Nucleic Acids Res.* **47**, 4026–4038 (2019).
33. Zhu, W. *et al.* Mcm10 and And-1/CTF4 recruit DNA polymerase α to chromatin for initiation of DNA replication. *Genes Dev.* **21**, 2288–2299 (2007).
34. Ercilla, A. *et al.* Physiological Tolerance to ssDNA Enables Strand Uncoupling during DNA Replication. *Cell Rep.* **30**, 2416-2429.e7 (2020).
35. Pugliese, G. M. *et al.* Inducible SMARCAL1 knockdown in iPSC reveals a link between replication stress and altered expression of master differentiation genes. *Dis. Model. Mech.* **12**, dmm039487 (2019).
36. Lemaçon, D. *et al.* MRE11 and EXO1 nucleases degrade reversed forks and elicit MUS81-dependent fork rescue in BRCA2-deficient cells. *Nat. Commun.* **8**, 860 (2017).
37. Murfuni, I. *et al.* Survival of the Replication Checkpoint Deficient Cells Requires MUS81-RAD52 Function. *PLoS Genet.* **9**, e1003910 (2013).

38. Blandino, F. *et al.* Phosphorylation status of MUS81 is a modifier of Olaparib sensitivity in BRCA2-deficient cells. *Nucleic Acids Res.* **51**, 6723–6737 (2023).
39. Kolinjivadi, A. M. *et al.* Smarcal1-Mediated Fork Reversal Triggers Mre11-Dependent Degradation of Nascent DNA in the Absence of Brca2 and Stable Rad51 Nucleofilaments. *Mol. Cell* **67**, 867-881.e7 (2017).
40. Huang, F. *et al.* Identification of specific inhibitors of human RAD51 recombinase using high-throughput screening. *ACS Chem. Biol.* **6**, 628–635 (2011).
41. Adolph, M. B. *et al.* RADX controls RAD51 filament dynamics to regulate replication fork stability. *Mol. Cell* **81**, 1074-1083.e5 (2021).
42. Zellweger, R. *et al.* Rad51-mediated replication fork reversal is a global response to genotoxic treatments in human cells. *J. Cell Biol.* **208**, 563–579 (2015).
43. Pellegrini, L. *et al.* Insights into DNA recombination from the structure of a RAD51-BRCA2 complex. *Nature* **420**, 287–293 (2002).
44. Wang, A. T. *et al.* A Dominant Mutation in Human RAD51 Reveals Its Function in DNA Interstrand Crosslink Repair Independent of Homologous Recombination. *Mol. Cell* **59**, 478–490 (2015).
45. Xu, Y. *et al.* 53BP1 and BRCA1 control pathway choice for stalled replication restart. *eLife* **6**, e30523 (2017).
46. Wray, J., Liu, J., Nickoloff, J. a. & Shen, Z. Distinct RAD51 associations with RAD52 and BCCIP in response to DNA damage and replication stress. *Cancer Res.* **68**, 2699–2707 (2008).
47. Carley, A. C. *et al.* Replication Protein A Phosphorylation Facilitates RAD52-Dependent Homologous Recombination in BRCA-Deficient Cells. *Mol. Cell. Biol.* **42**, e0052421 (2022).
48. Lukac, D., Machacova, Z. & Moudry, P. Emetine blocks DNA replication via proteosynthesis inhibition not by targeting Okazaki fragments. *Life Sci. Alliance* **5**, e202201560 (2022).
49. Cong, K. & Cantor, S. B. Exploiting replication gaps for cancer therapy. *Mol. Cell* **82**, 2363–2369 (2022).

50. González-Acosta, D. *et al.* PrimPol-mediated repriming facilitates replication traverse of DNA interstrand crosslinks. *EMBO J.* 1–17 (2021) doi:10.15252/embj.2020106355.

51. Taylor, M. R. G. & Yeeles, J. T. P. The Initial Response of a Eukaryotic Replisome to DNA Damage. *Mol. Cell* **70**, 1067-1080.e12 (2018).

52. Abe, T. *et al.* AND-1 fork protection function prevents fork resection and is essential for proliferation. *Nat. Commun.* **9**, 3091 (2018).

53. Gambus, A. *et al.* A key role for Ctf4 in coupling the MCM2-7 helicase to DNA polymerase α within the eukaryotic replisome. *EMBO J.* **28**, 2992–3004 (2009).

54. Errico, A. *et al.* Tipin/Tim1/And1 protein complex promotes Pol alpha chromatin binding and sister chromatid cohesion. *EMBO J.* **28**, 3681–3692 (2009).

55. Hashimoto, Y., Puddu, F. & Costanzo, V. RAD51- and MRE11-dependent reassembly of uncoupled CMG helicase complex at collapsed replication forks. *Nat. Struct. Mol. Biol.* **19**, 17–24 (2011).

56. Mann, A. *et al.* POLθ prevents MRE11-NBS1-CtIP-dependent fork breakage in the absence of BRCA2/RAD51 by filling lagging-strand gaps. *Mol. Cell* **82**, 4218-4231.e8 (2022).

57. Petermann, E., Orta, M. L., Issaeva, N., Schultz, N. & Helleday, T. Hydroxyurea-Stalled Replication Forks Become Progressively Inactivated and Require Two Different RAD51-Mediated Pathways for Restart and Repair. *Mol. Cell* **37**, 492–502 (2010).

58. Lambert, S. *et al.* Homologous recombination restarts blocked replication forks at the expense of genome rearrangements by template exchange. *Mol. Cell* **39**, 346–359 (2010).

59. Mason, J. M., Chan, Y.-L., Weichselbaum, R. W. & Bishop, D. K. Non-enzymatic roles of human RAD51 at stalled replication forks. *Nat. Commun.* **10**, 4410 (2019).

60. Naiman, K. *et al.* Replication dynamics of recombination-dependent replication forks. *Nat. Commun.* **12**, 923 (2021).

61. Cotta-Ramusino, C. *et al.* Exo1 processes stalled replication forks and counteracts fork reversal in checkpoint-defective cells. *Mol. Cell* **17**, 153–159 (2005).

62. Bansbach, C. E., Bétous, R., Lovejoy, C. a., Glick, G. G. & Cortez, D. The annealing helicase SMARCAL1 maintains genome integrity at stalled replication forks. *Genes Dev.* **23**, 2405–2414 (2009).

63. Belan, O. *et al.* POLQ seals post-replicative ssDNA gaps to maintain genome stability in BRCA-deficient cancer cells. *Mol. Cell* **82**, 4664-4680.e9 (2022).

64. Schlacher, K. *et al.* Double-Strand Break Repair-Independent Role for BRCA2 in Blocking Stalled Replication Fork Degradation by MRE11. *Cell* **145**, 529–542 (2011).

65. Tong, D. *et al.* Rad52 gene mutations in breast/ovarian cancer families and sporadic ovarian carcinoma patients. *Oncol. Rep.* **10**, 1551–3 (2003).

66. Chandramouly, G. *et al.* Small-Molecule Disruption of RAD52 Rings as a Mechanism for Precision Medicine in BRCA-Deficient Cancers. *Chem. Biol.* **22**, 1491–1504 (2015).

67. Hengel, S. R. *et al.* Small-molecule inhibitors identify the RAD52-ssDNA interaction as critical for recovery from replication stress and for survival of BRCA2 deficient cells. *eLife* **5**, (2016).

68. He, Q. *et al.* Structures of the human CST-Polα-primase complex bound to telomere templates. *Nature* **608**, 826–832 (2022).

69. Grimme, J. M. *et al.* Human Rad52 binds and wraps single-stranded DNA and mediates annealing via two hRad52-ssDNA complexes. *Nucleic Acids Res.* **38**, 2917–2930 (2010).

70. Subramanyam, S., Ismail, M., Bhattacharya, I. & Spies, M. Tyrosine phosphorylation stimulates activity of human RAD51 recombinase through altered nucleoprotein filament dynamics. *Proc. Natl. Acad. Sci.* **113**, 201604807 (2016).

71. Pirzio, L. M., Pichierri, P., Bignami, M. & Franchitto, A. Werner syndrome helicase activity is essential in maintaining fragile site stability. *J. Cell Biol.* **180**, 305–314 (2008).

FIGURE LEGENDS

Fig. 1 - RAD52 deficiency stimulates repriming. a. Analysis of parental ssDNA exposure by immunofluorescence. MRC5 WT were treated as indicated on the experimental scheme above. For untreated cells, Epigallocatechin (RAD52i, 50 μM) was kept for 4 hours. After the exposure to 2 mM hydroxyurea (HU), replication recovery was given by adding fresh medium. The ssDNA was detected by IdU immunofluorescence. Graph shows the intensity of ssDNA staining (AU) per cell from three replicates. Representative images are shown. Scale bar represents 10 μm. **b and c.** Effect of Mirin on parental ssDNA exposure. U2OS WT were treated with 4h HU as indicated in A (B) or with 0.5 mM HU (C). Graph shows the intensity of ssDNA staining (AU). Representative images are shown. Scale bar represents 10 μm. **c.** Detection of ssDNA gaps in U2OS through S1 fibers assay. On top: schemes describing the experiment. Cells were treated with or without the S1 nuclease before spreading of DNA fibers. The graph reports the IdU/CldU ratio for each DNA fiber. Representative images of single DNA fibers are shown. Scale bar represents 5 μm. All the values above are presented as means ± SE (ns = not significant; *P < 0.1; **P<0.1; ***P < 0.001; ****P < 0.0001; Kruskal-Wallis test).

Fig. 2 – Parental DNA gaps are Polα-, but not PrimPol-, dependent in the absence of RAD52. a. Analysis of ssDNA gaps through S1 fiber assay. Wild-type MRC5 or KO PrimPol were treated with 0.5 μM HU for 4 hours. RAD52i was given 30 min before replicative stress induction. The graph reports the mean IdU/CldU ratio. **b.** Analysis of PrimPol-ssDNA interaction using Proximity Ligation Assay (PLA). MRC5 -/- PrimPol were transfected with peGFP-PrimPol WT. 24 hours after transfection, cells were treated with 100 μM IdU for 20 hours, released for 2 hours in fresh medium and subjected to RAD52i and HU (0.5 mM). To assess PrimPol-ssDNA association, the PLA reaction was carried out using antibodies against GFP and IdU. Controls were subjected to PLA with anti-IdU or anti-GFP only. The graph reports the number of PLA spot per nucleus. Representative images are shown. **c.** Analysis of PrimPol recruitment on DNA by chromatin fractionation. MRC5 KO PrimPol were transfected with peGFP-PrimPol WT. After 48 hours from transfection, cells were treated with RAD52i and HU (0.5 mM) for 2 and 4 hours. Cell pellets were subjected to chromatin fractionation and the protein extracts were quantified by Western Blotting. PrimPol was identified by using an antibody directed against GFP. The whole cell extracts was used as control (INPUT). **d.** Analysis of Polα-parental ssDNA interaction by PLA. U2OS WT were treated with 100 μM IdU for 20 hours, released for 2 hours in fresh medium and subjected to RAD52i and HU (0.5 mM). The PLA reaction was carried out using antibodies against the POLA1 Polα subunit and IdU. The graph reports the number of PLA spot per nucleus. The control was subjected to PLA with the anti-Polα alone. Representative images are shown. **e.** Analysis of parental ssDNA exposure in Polα-inhibited cells. U2OS WT were treated as indicated on the experimental scheme. ST1926 (Polαi) was given at 0.3 μM. Graph represents the IdU intensity (AU) per cell. Representative images are reported. **f.** Analysis of ssDNA gaps through S1 fiber assay. Wild-type MRC5 or MRC5 KO PrimPol were treated with Polαi (0.3 μM) and RAD52i 30 min before HU (0.5 mM; 4h). The graph shows the mean IdU/CldU ratio. (ns = not

significant; *P < 0.1; **P<0.1; ***P < 0.001; ****P < 0.0001; Mann–Whitney test;). Scale bars represent 10 µm.

Fig. 3 - Polα recruitment under RAD52 deficiency depends on replication fork remodelling. a. Analysis of Polα - parental ssDNA interaction by PLA in U2OS shSMARCAL1. SMARCAL1 silencing was induced by giving Doxycycline (Dox) 24 hours before treatment with IdU for 20 hours. The cells were then released for 2 hours in fresh medium and treated with or without RAD52i 30 min before giving HU (2 mM). PLA reaction was carried out using antibodies against POLA1 and IdU. Graph shows the number of PLA spot per nucleus. Representative images are shown. **b**. Analysis of Polα recruitment at DNA through chromatin fractionation. U2OS shSMARCAL1 were treated as described above. Polα was identified by using an antibody directed against the Polα subunit POLA1, and LAMIN B1 used as loading control. A graph of POLA1/LAMIN B1 quantification from 3 replicates is reported below **c.** Analysis of Polα-parental ssDNA in U2OS WT. Cells were treated with IdU for 20 hours, released 2 hours in fresh medium, and subjected to RAD52i and MIRIN before giving HU (2 mM). PLA reaction was carried out using antibodies against POLA1 and IdU. The graph reports the number of PLA spot per nucleus. Representative images are shown. (ns = not significant; *P < 0.1; **P<0.1; ***P < 0.001; ****P < 0.0001; Kruskal-Wallis test;). Scale bars represent 10 µm.
d. Analysis of Polα-parental ssDNA interaction in U2OS WT or transfected with BRCA2 siRNA. Western blot showsBRCA2 expression level after silencing with the siRNA. After IdU labelling, cells were treated with MIRIN and HU (2 mM). PLA reaction was carried out using antibodies against POLA1 and IdU. Graph shows the number of PLA spots per nucleus. Representative images are shown. **e.** Western blot showing BRCA2 and GFP expression level. LAMIN B1 was used as loading control. **f.** Analysis of PrimPol-parental ssDNA association by PLA. MRC5 KO PrimPol were transfected with peGFP-PrimPol WT. On the same day, cells were transfected with the BRCA2 siRNA. 24 hours after transfections, cells were treated with IdU for 20 hours, released for 2 hours in fresh medium and subjected to RAD52i or MIRIN and HU (0.5 mM). Graph shows the number of PLA spots per nucleus. **g.** Analysis of Polα-parental ssDNA interaction in MRC5 shBRCA2 and MUS81 KO. BRCA2 silencing was obtained by treating the cells with Dox (1µg/ml) 48 hours before HU (2 mM) exposure. BRCA2 silencing was confirmed by qRT–PCR analysis (See Fig. S11). PLA reaction was carried out using antibodies against POLA1 and IdU. Graph shows the number of PLA spots per nucleus. (ns = not significant; *P < 0.1; **P<0.1; ***P < 0.001; ****P < 0.0001; Kruskal-Wallis test;). Scale bars represent 10 µm.

Fig. 4 – RAD52 inhibition increases Polα-RAD51 association. a. Analysis of Polα-RAD51 association by PLA in U2OS WT. Cells were subjected to RAD52i 30 min before HU (2 mM) treatment. PLA reaction was carried out using antibodies against POLA1 and RAD51. The graph shows the number of PLA spot per nucleus. The control was subjected to PLA with only one primary antibody. Representative images are shown. Scale bar represents 10 µm **b.** Analysis of Polα-RAD51 association by PLA in U2OS WT. Cells were exposed to RAD52i 20 min before HU (0.5 mM) treatment of 2 and 4 hours. PLA reaction was carried out using antibodies against POLA1 and RAD51. The graph shows the

number of PLA spot per nucleus. **c.** Experimental scheme of super-resolution (SR) microscopy assay. **d.** Quantification of EdU-RAD51-Polα interaction by SR microscopy (dSTORM). U2OS WT were treated as indicated on the panel C. The graph represents the percentage of variation in co-localization events of EdU-RAD51, EdU- Polα and EdU-RAD51-Polα. **e.** Representative dSTORM images of two nuclei immunolabeled for nascent DNA (cyan), Polα (magenta) and RAD51 (yellow). Scale bars = 20µm, 1µm and 100nm. A representative sketch of a common topology of the 3 signal is also shown. All the values above are presented as means ± SE (ns = not significant; *P < 0.1; **P<0.1; ***P < 0.001; ****P < 0.0001; Kruskal-Wallis test;).

Fig. 5 - Polα engagement is mediated by RAD51. a. Analysis of Polα-parental ssDNA association by PLA. U2OS WT were treated with IdU for 20 hours, released for 2 hours in fresh DMEM and successively treated with or without RAD52i and RAD51i 30 min before HU (2 mM). The graph shows the number of PLA spot per nucleus. Representative images are shown. **b.** Analysis of Polα recruitment at the DNA by chromatin fractionation. MRC5 WT were treated with RAD52i and RAD51i 30 min before HU (2mM). Polα was identified by using an antibody directed against the Polα subunit POLA1. The whole cell extracts was used as control (INPUT). A graph of POLA1/LAMIN B1 quantification from 3 replicates is reported below. **c.** Western blot and quantification graph showing the level of RAD51 expression in RAD51 siRNA J11-transfected cells (2 pmol and 20 pmol). **d.** Analysis of Polα-parental ssDNA association by PLA in U2OS WT. Cells were transfected with the RAD51 siRNA (J11) at 2 pmol and 20 pmol 24 hours before 20 hours of IdU labelling. After 2 hours of release in fresh medium, cells were treated with RAD52i 30 min before giving HU (2 mM). PLA reaction was carried out using antibodies against POLA1 and IdU. The graph reports the number of PLA spot per nucleus. Representative images are shown. **e**. Analysis of Polα-parental ssDNA association by PLA. U2OS WT were treated as indicated by the experimental scheme above. The graph shows the number of PLA spot per nucleus. Representative images are reported. All the values above are presented as means ± SE (ns = not significant; *P < 0.1; **P<0.1; ***P < 0.001; ****P < 0.0001; Kruskal–Wallis test;). Scale bars represent 10 µm.

Fig. 6 - RPA and RAD51 differentially regulate Polα/Primase activities.
a, RAD51 titration on Polα/Primase *de novo* RNA synthesis on dT70 mer templates, with products labelled with [α-^{32}P]ATP. Size markers are synthesized Cy3-labelled poly(dT) ssDNA with a length of 10, 20, 40 and 60. **b**, Model depicting the observed elongated RNA products in the presence of RAD51 (orange circle). Polα–primase (yellow circle labeled as α) binds the template poly(dT)70 and synthesize RNA primer (red) that length could be modulated by RAD51. **c**, Quantification of RNA products in the experiment directly above. 10 and 20 nt RNA priming product (grey), template size RNA product (green) and long RNA product that is stacked in the well (red). **d**, RPA titration on Polα/Primase *de novo* RNA synthesis on dT70 mer templates, with products labelled with [α-^{32}P]ATP. **e**, Model depicting the observed elongated RNA products in the presence of RPA (green square). Polα–primase (yellow circle labeled as α) binds the template poly(dT)70 and synthesize RNA primer (red) while its activity are attenuated in the presence of RPA. **f**, Quantification

of RNA products in the experiment directly above. 10 and 20 nt RNA priming product (grey) and long RNA product (red). **g-l**, Same as **a-f** except using long circular ssDNA (φX174 Virion DNA) as a template instead of poly(dT)70. Polα/Primase no longer generate 70 nt RNA product in the presence of RAD51. **m** and **n**, The 5'-Cy3-labeled poly-rA_{15} primer was extended by DNA synthesis activity of Polα/Primase in the presence of dATP and on RAD51 (**m**) and RPA (**n**) titration. Size markers are synthesized Cy3-labelled poly(dT) ssDNA.

Fig. 7 - Polα recruitment occurs downstream extensive replication fork degradation. **a.** Experimental scheme of single-cell assay for in situ Protein Interaction (SIRF). **b.** Analysis of Polα-nascent ssDNA interaction by SIRF. U2OS WT were treated as indicated above. The model on the left represents the expected background. SIRF reaction was carried out after the Click-iT™ reaction by using antibodies against POLA1 and biotin.The graph shows the mean number of SIRF spots per nucleus only of cells subjected to 5 minutes of recovery from EdU labelling. Where present, the representative images are shown above the graph. Controls were subjected to SIRF with anti-biotin only. **c.** Analysis of Polα-nascent ssDNA interaction by SIRF. U2OS WT were treated as indicated above. SIRF reaction was carried out after the Click-iT™ reaction by using antibodies against POLA1 and biotin. The graph shows the number of SIRF spots per nucleus only of cells subjected to 15 minutes of recovery from EdU labelling. Where present, the representative images are shown above the graph. **d**. Analysis of RAD51-nascent DNA interaction by SIRF in U2OS shBRCA2. Cells were exposed to EdU labelling during all the HU treatment. SIRF reaction was carried out using antibodies against RAD51 and biotin. The graph shows the mean number of SIRF spots per cell. BRCA2 silencing was induced by giving Dox (1μg/ml) 48 hours before the experiment. BRCA2 silencing was confirmed by qRT–PCR analysis of BRCA2 mRNA level 48 hours after doxycycline induction (See suppl. Fig 11). **e.** Analysis of RAD52-parental ssDNA interaction by PLA. U2OS WT were treated with IdU for 20 hours. After a release of 2 hours in fresh medium, cells were subjected to Polαi (ST1926, 1 μM) alone or combined with HU (0.5 or 2 mM; 2h). PLA reaction was carried out using antibodies against RAD52 and IdU. Graph shows the number of PLA spots per nucleus. Controls were subjected to PLA with anti-RAD52 only. Representative images are shown. Means ± SE are reported in scatter plots (ns = not significant; *P < 0.1; **P<0.1; ***P < 0.001; ****P < 0.0001; Kruskal–Wallis test;). Scale bars represent 10 μm.

Fig. 8 - Polα-repriming prevents DSBs formation and chromosomal aberrations in RAD52 deficient cells. **a.** DSBs detection by immunofluorescence. U2OS WT were treated for 4h with HU and inhibitors, and recovered for 18h in drug-free medium before analysis. Immunofluorescence was carried out by using an antibody against γH2AX. The graph shows the percentage of γH2AX positive cells. Representative images are shown. **b.** Analysis of chromosomal aberrations in MRC5SV40 cells treated as in the experimental scheme above. The graphs show the mean of total chromosomal aberrations per cell and the mean of chromosomal breaks (**c**) and complex chromosomal aberrations per cell (**d**). Representative images of Giemsa-stained metaphases are given. Red arrows indicate chromosomal breaks; Framed in blue are shown other chromosomal aberrations and

chromosomal exchanges. Insets show a magnification of the marked chromosome. **e.** 53BP1 NBs detection. Cells were treated as indicated in the experimental scheme above. Immunofluorescence was carried out by using an antibody against 53BP1. The graph shows the number of cells presenting 53BP1 NBs (0, 0-10 or >10). All the values above are presented as means ± SE (ns = not significant; *P < 0.1; **P<0.1; ***P < 0.001; ****P < 0.0001; ANOVA test;). Scale bars represent 10 µm. **f.** Model describing the RAD51-dependent Polα recruitment and gap formation downstream extensive degradation triggered by RAD52 deficiency.

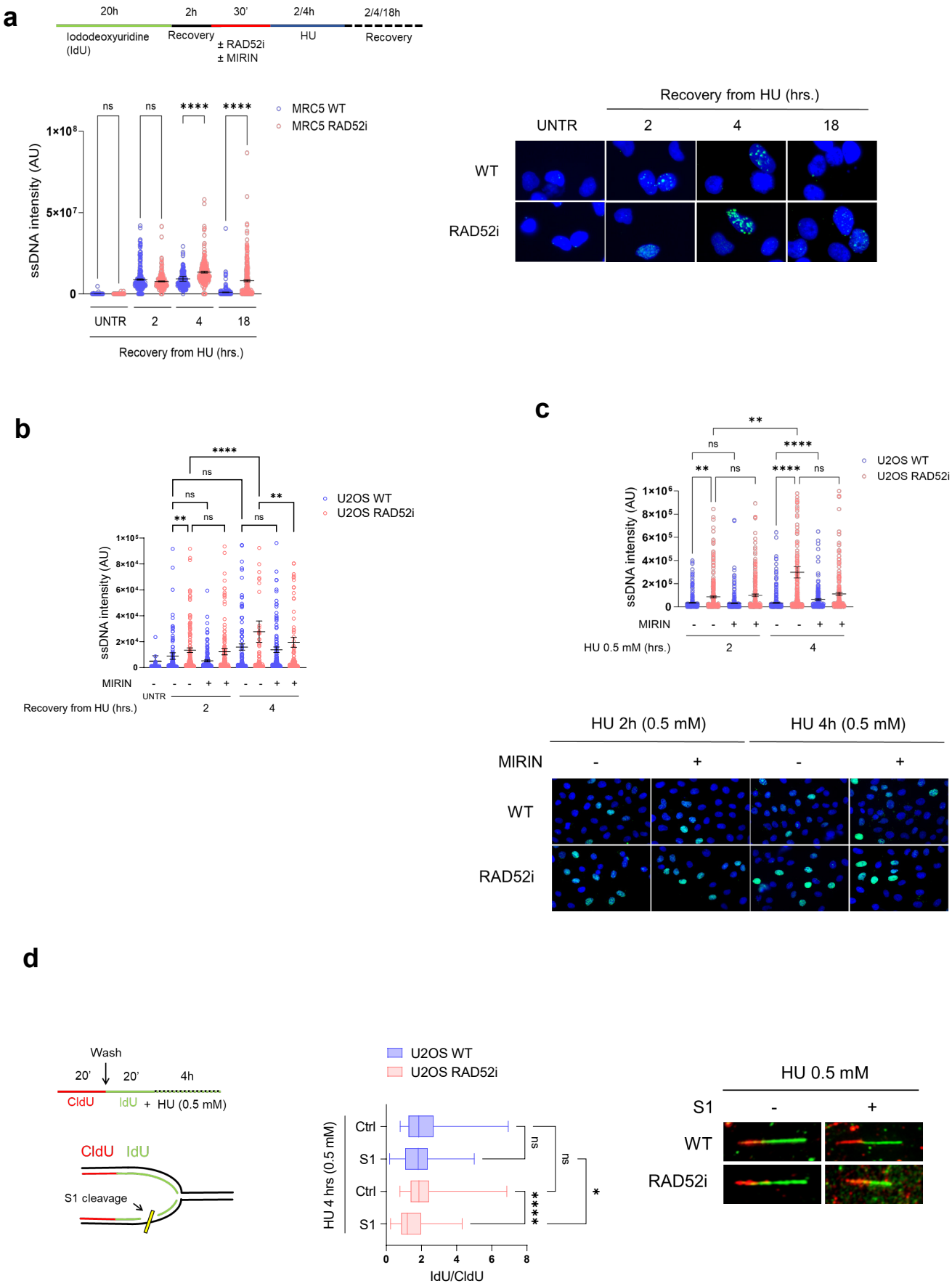
a
20h
2h
30'
2/4h
2/4/18h
Iododeoxyuridine (IdU)
Recovery
± RAD52i
± MIRIN
HU
Recovery
MRC5 WT
MRC5 RAD52i
ssDNA intensity (AU)
Recovery from HU (hrs.)
UNTR
2
4
18
WT
RAD52i
b
U2OS WT
U2OS RAD52i
MIRIN
c
HU 0.5 mM (hrs.)
HU 2h (0.5 mM)
HU 4h (0.5 mM)
d
Wash
CldU
IdU + HU (0.5 mM)
S1 cleavage
HU 4 hrs (0.5 mM)
Ctrl
S1
IdU/CldU
HU 0.5 mM

Figure 1

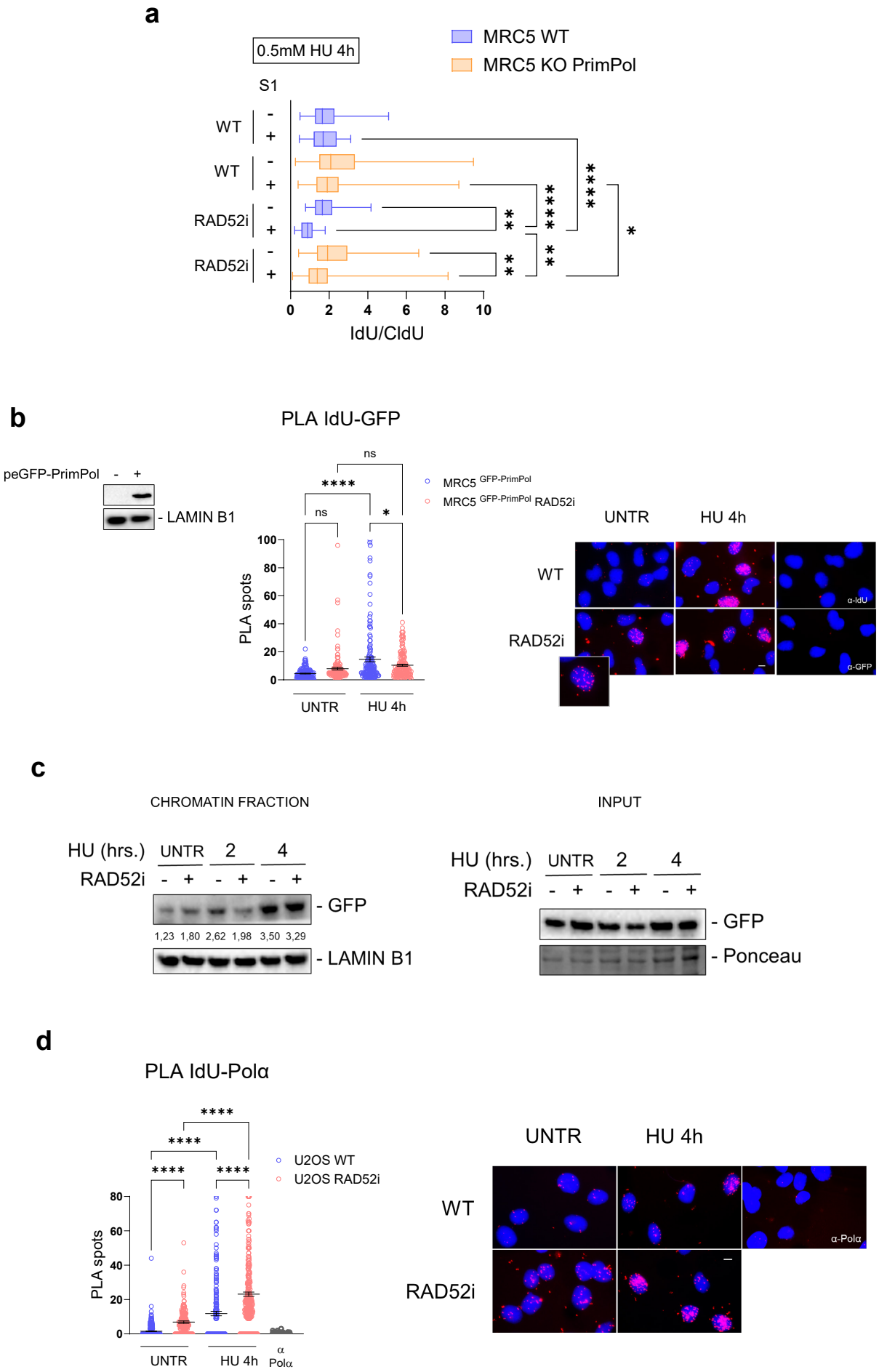
a
0.5mM HU 4h
MRC5 WT
MRC5 KO PrimPol
S1
WT
WT
RAD52i
RAD52i
IdU/CldU
b
PLA IdU-GFP
peGFP-PrimPol
LAMIN B1
PLA spots
MRC5 GFP-PrimPol
MRC5 GFP-PrimPol RAD52i
UNTR
HU 4h
WT
RAD52i
α-IdU
α-GFP
c
CHROMATIN FRACTION
INPUT
HU (hrs.)
RAD52i
GFP
LAMIN B1
Ponceau
1,23 1,80 2,62 1,98 3,50 3,29
d
PLA IdU-Polα
U2OS WT
U2OS RAD52i
PLA spots
UNTR
HU 4h
α Polα
WT
RAD52i
α-Polα

Figure 2

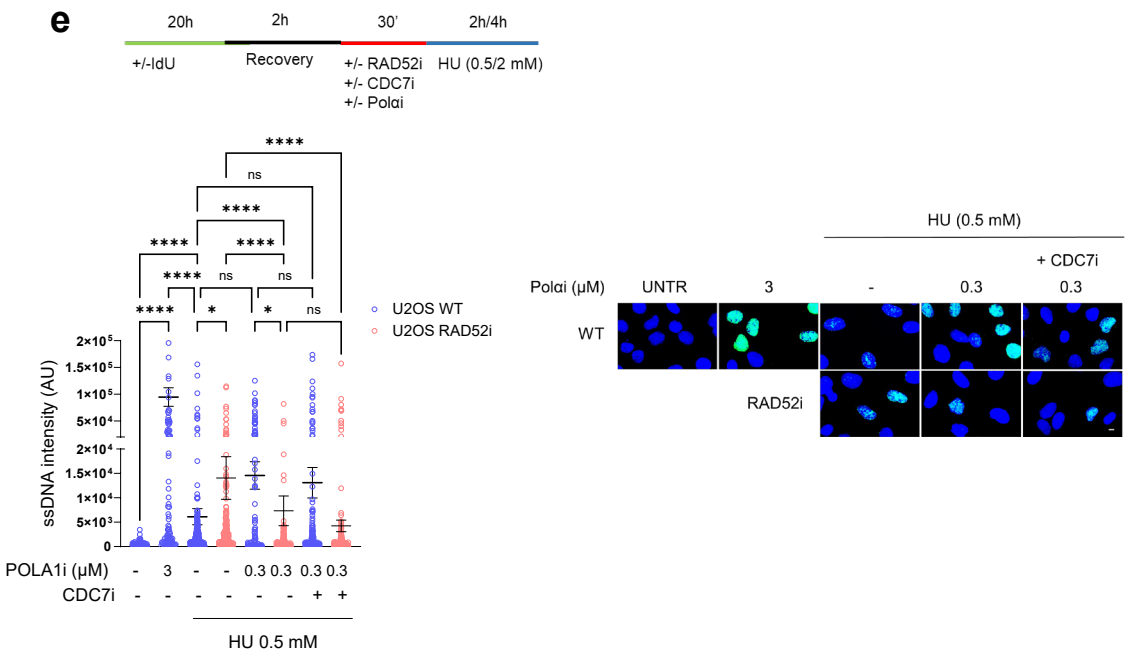

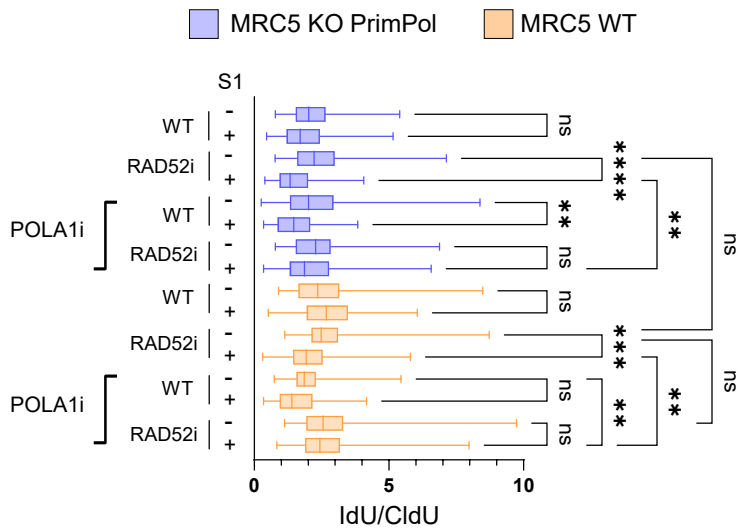

Figure 2 cont'd

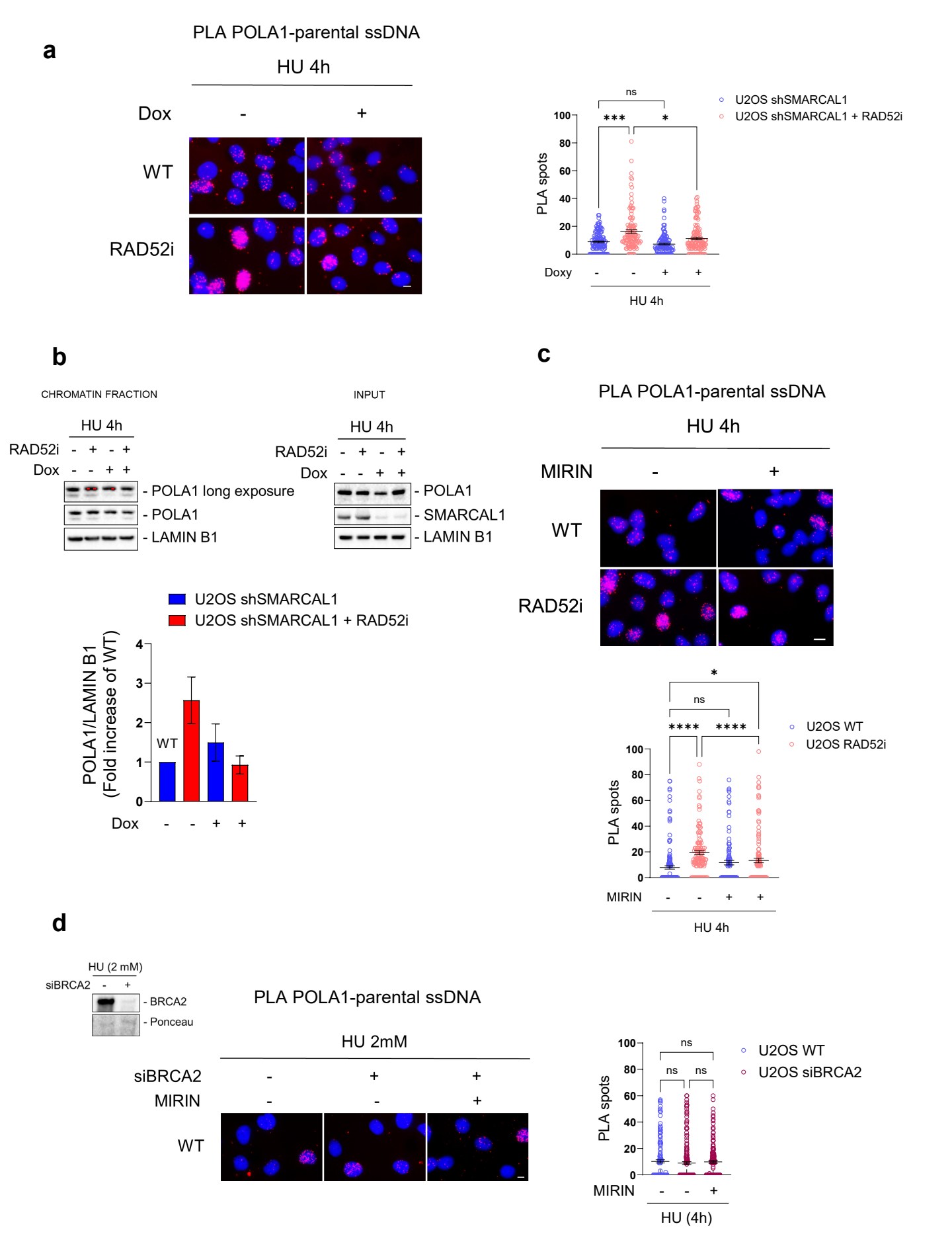
a
PLA POLA1-parental ssDNA
HU 4h
Dox
-
+
WT
RAD52i
ns
***
*
U2OS shSMARCAL1
U2OS shSMARCAL1 + RAD52i
PLA spots
100
80
60
40
20
0
Doxy
- - + +
HU 4h
b
CHROMATIN FRACTION
INPUT
HU 4h
RAD52i - + - +
Dox - - + +
- POLA1 long exposure
- POLA1
- LAMIN B1
- SMARCAL1
U2OS shSMARCAL1
U2OS shSMARCAL1 + RAD52i
POLA1/LAMIN B1
(Fold increase of WT)
4
3
2
1
0
WT
Dox - - + +
c
PLA POLA1-parental ssDNA
HU 4h
MIRIN
-
+
WT
RAD52i
*
ns
****
****
U2OS WT
U2OS RAD52i
PLA spots
MIRIN - - + +
HU 4h
d
HU (2 mM)
siBRCA2 - +
- BRCA2
- Ponceau
PLA POLA1-parental ssDNA
HU 2mM
siBRCA2 - + +
MIRIN - - +
WT
ns
ns
ns
U2OS WT
U2OS siBRCA2
PLA spots
MIRIN - - +
HU (4h)

Figure 3

e

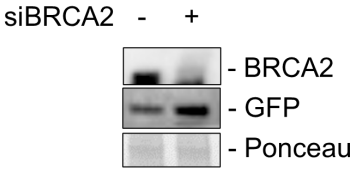

f

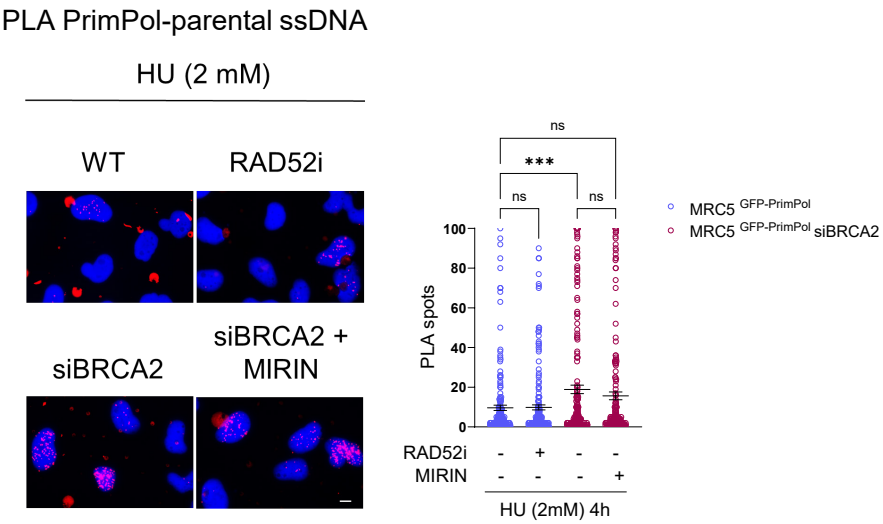

g

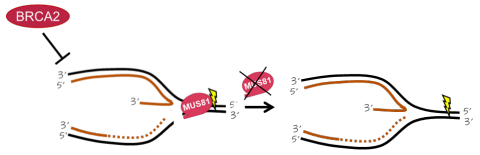

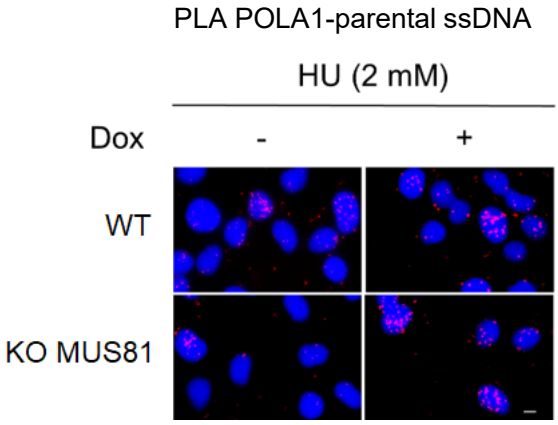

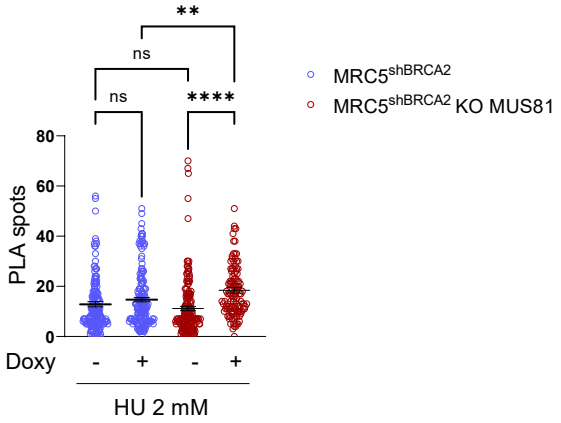

Figure 3 cont'd

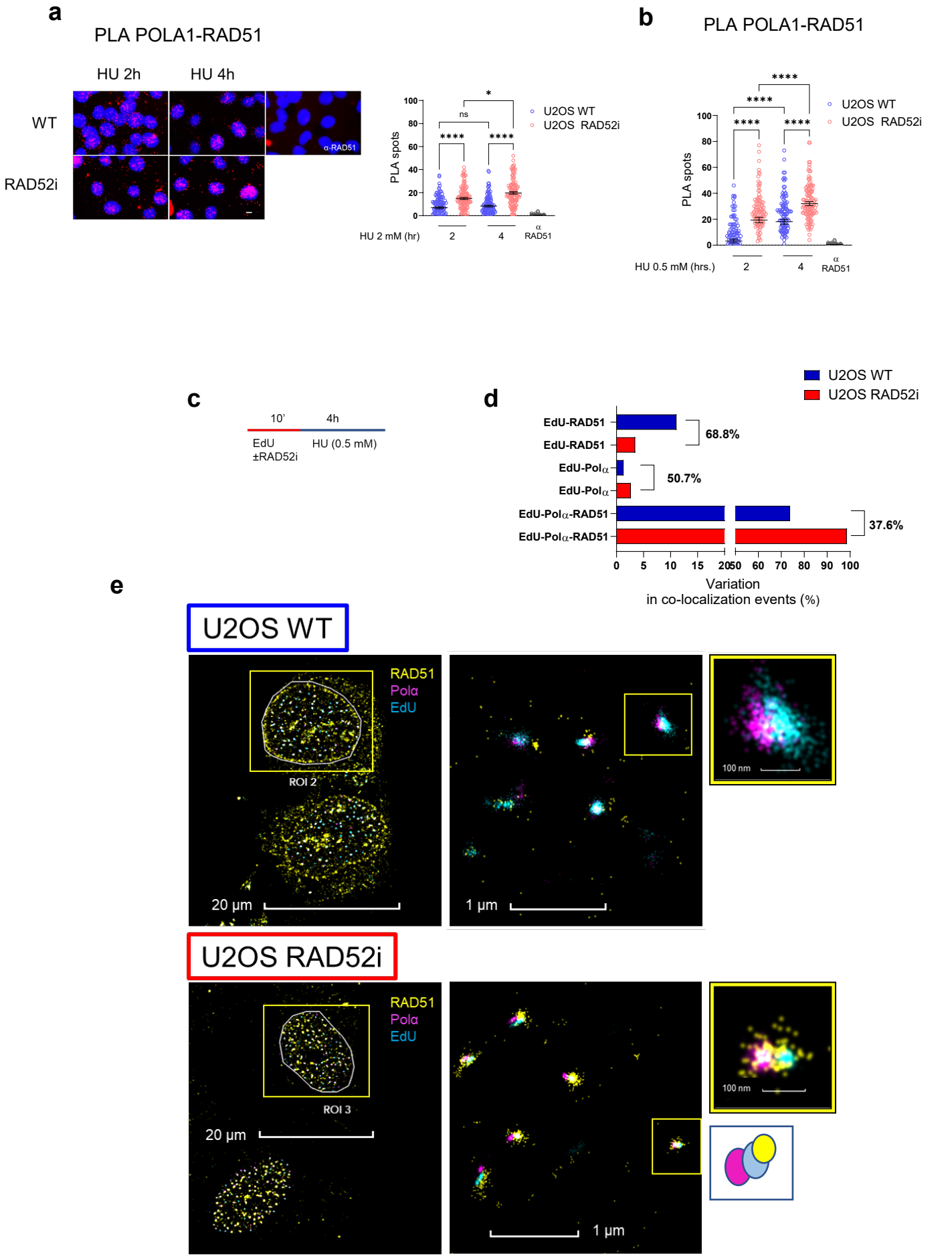
a
PLA POLA1-RAD51
HU 2h
HU 4h
WT
RAD52i
α-RAD51
PLA spots
U2OS WT
U2OS RAD52i
ns
*
****
HU 2 mM (hr)
2
4
α RAD51
b
PLA POLA1-RAD51
HU 0.5 mM (hrs.)
c
10'
4h
EdU ±RAD52i
HU (0.5 mM)
d
EdU-RAD51
EdU-Polα
EdU-Polα-RAD51
68.8%
50.7%
37.6%
Variation in co-localization events (%)
e
U2OS WT
RAD51
Polα
EdU
ROI 2
20 µm
1 µm
100 nm
U2OS RAD52i
ROI 3

Figure 4

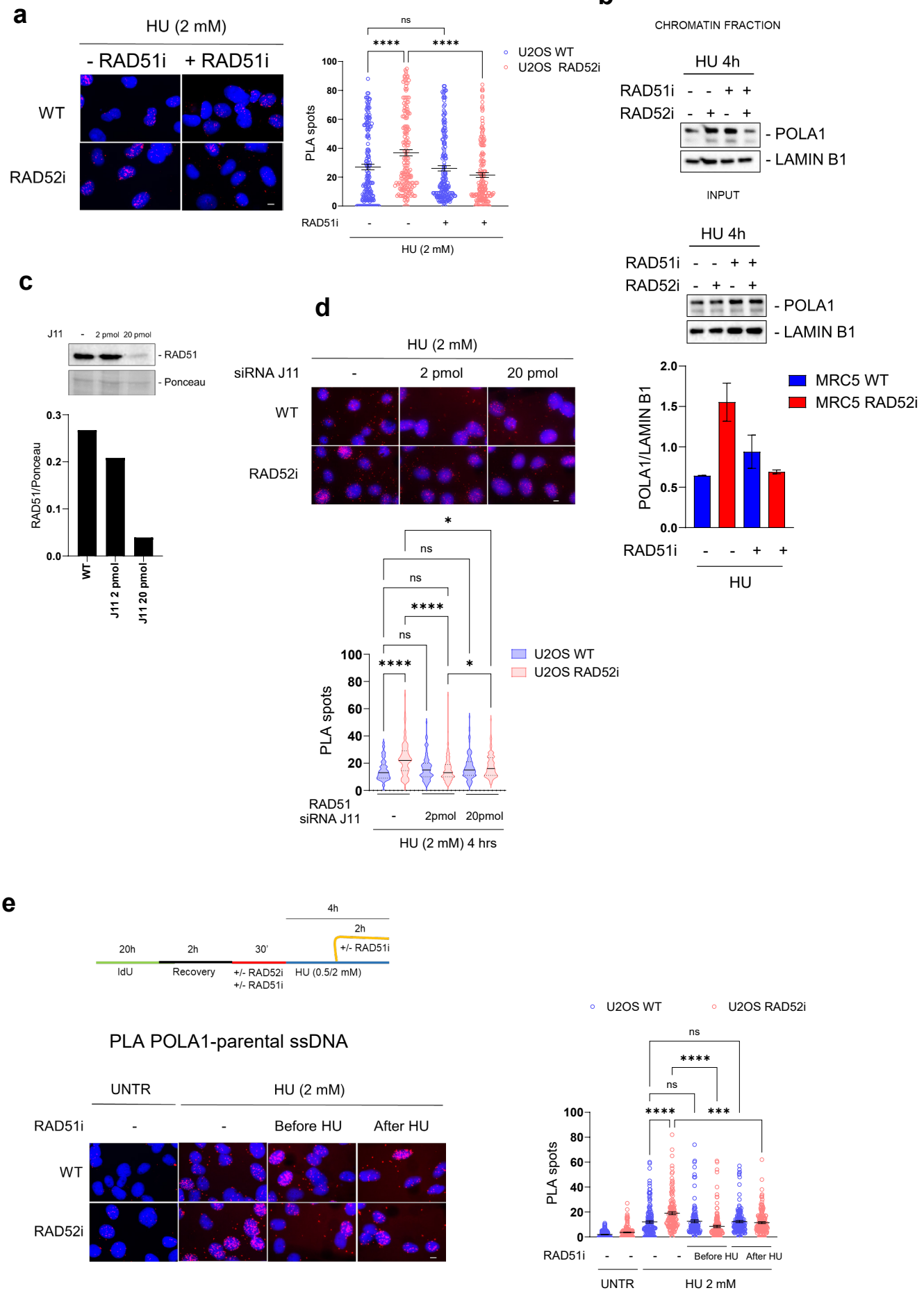
a
HU (2 mM)
- RAD51i
+ RAD51i
WT
RAD52i
PLA spots
U2OS WT
U2OS RAD52i
RAD51i
HU (2 mM)
b
CHROMATIN FRACTION
HU 4h
RAD51i
RAD52i
- POLA1
- LAMIN B1
INPUT
HU 4h
RAD51i
RAD52i
- POLA1
- LAMIN B1
POLA1/LAMIN B1
MRC5 WT
MRC5 RAD52i
RAD51i
HU
c
J11
2 pmol
20 pmol
- RAD51
- Ponceau
RAD51/Ponceau
WT
J11 2 pmol
J11 20 pmol
d
HU (2 mM)
siRNA J11
2 pmol
20 pmol
WT
RAD52i
PLA spots
U2OS WT
U2OS RAD52i
RAD51
siRNA J11
2pmol
20pmol
HU (2 mM) 4 hrs
e
4h
2h
20h
2h
30'
+/- RAD51i
IdU
Recovery
+/- RAD52i
+/- RAD51i
HU (0.5/2 mM)
PLA POLA1-parental ssDNA
UNTR
HU (2 mM)
RAD51i
Before HU
After HU
WT
RAD52i
U2OS WT
U2OS RAD52i
PLA spots
RAD51i
Before HU
After HU
UNTR
HU 2 mM

Figure 5

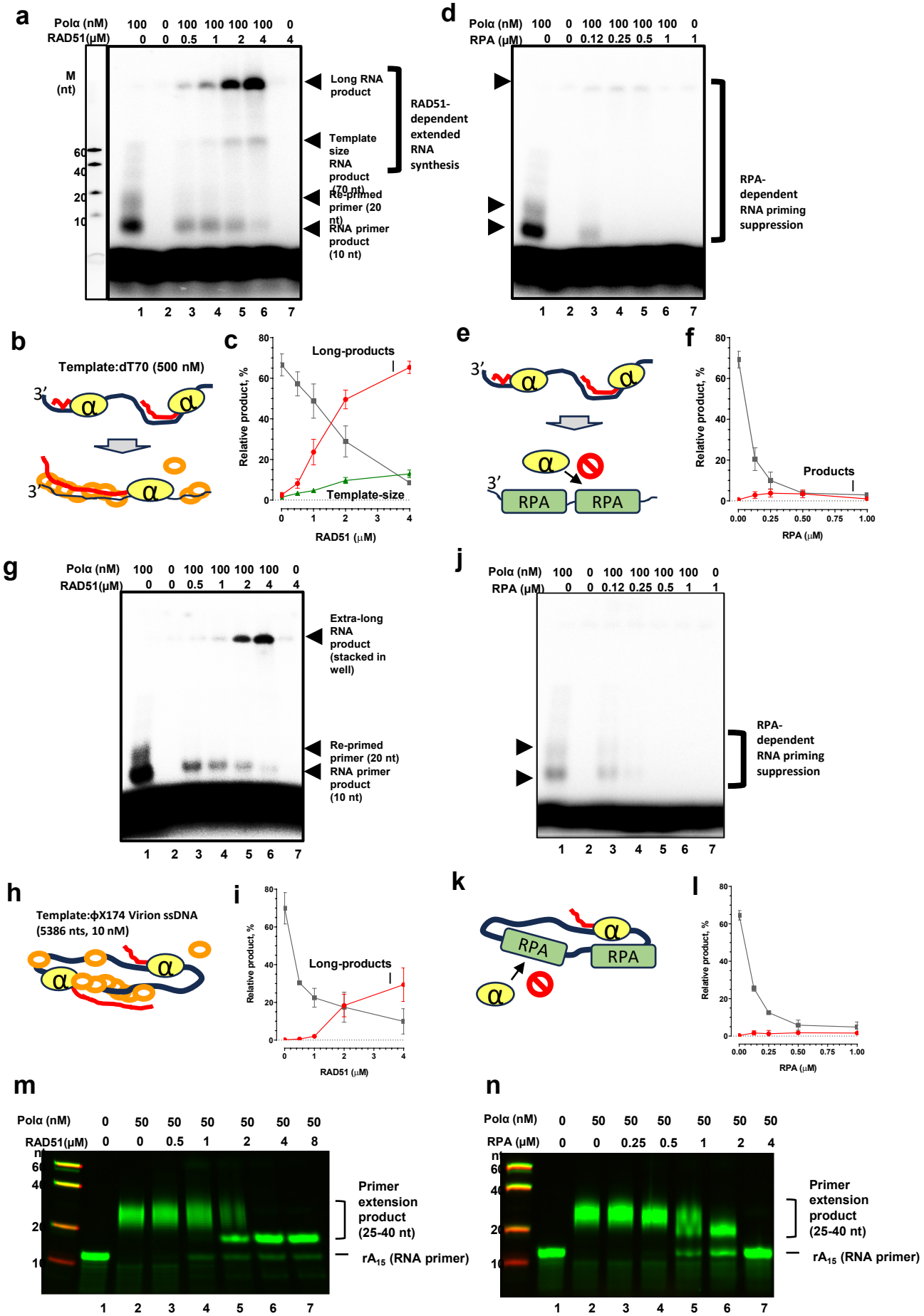

Figure 6: RPA and RAD51 differentially regulate Polα-primase activities

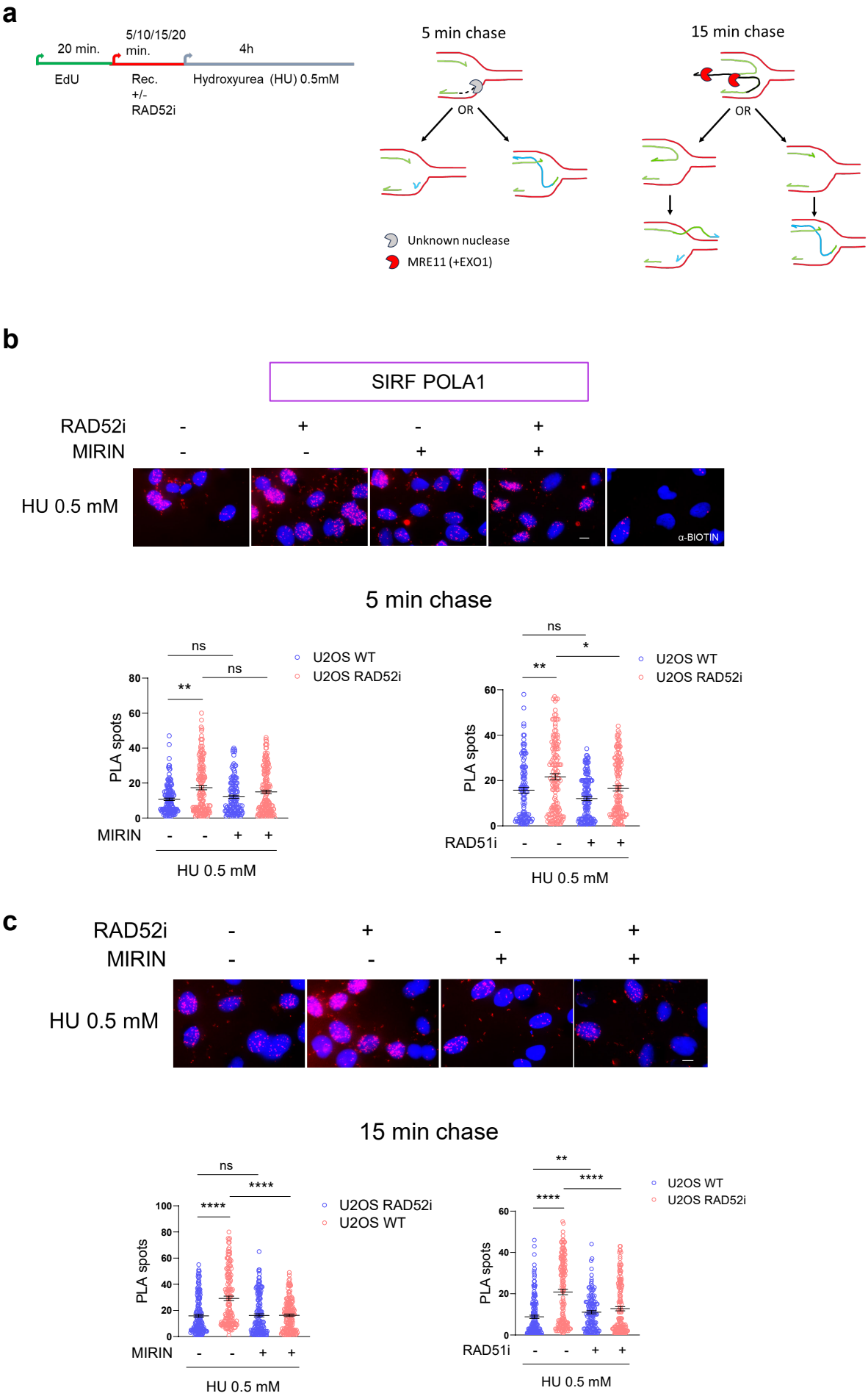
a
20 min.
5/10/15/20 min.
4h
EdU
Rec. +/- RAD52i
Hydroxyurea (HU) 0.5mM
5 min chase
15 min chase
OR
Unknown nuclease
MRE11 (+EXO1)
b
SIRF POLA1
RAD52i
MIRIN
HU 0.5 mM
α-BIOTIN
5 min chase
U2OS WT
U2OS RAD52i
PLA spots
MIRIN
RAD51i
HU 0.5 mM
ns
*
**
c
15 min chase
****

Figure 7

d

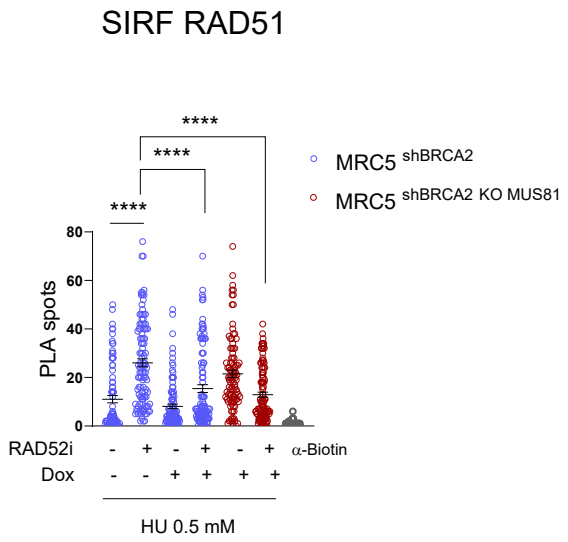

e

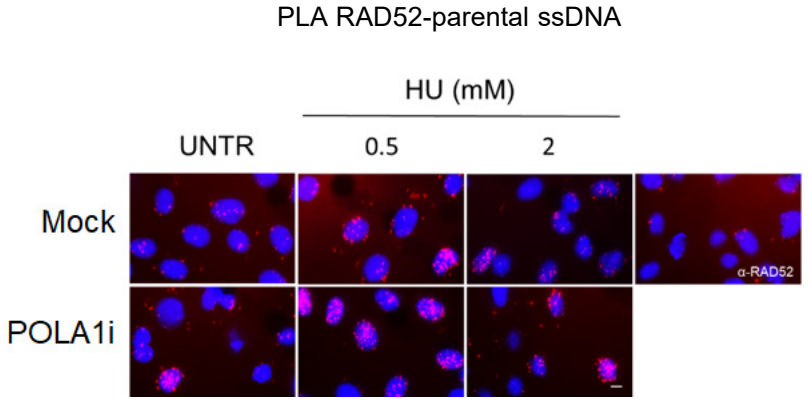

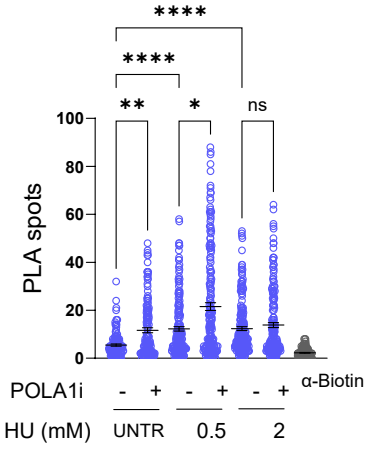

Figure 7 cont'd

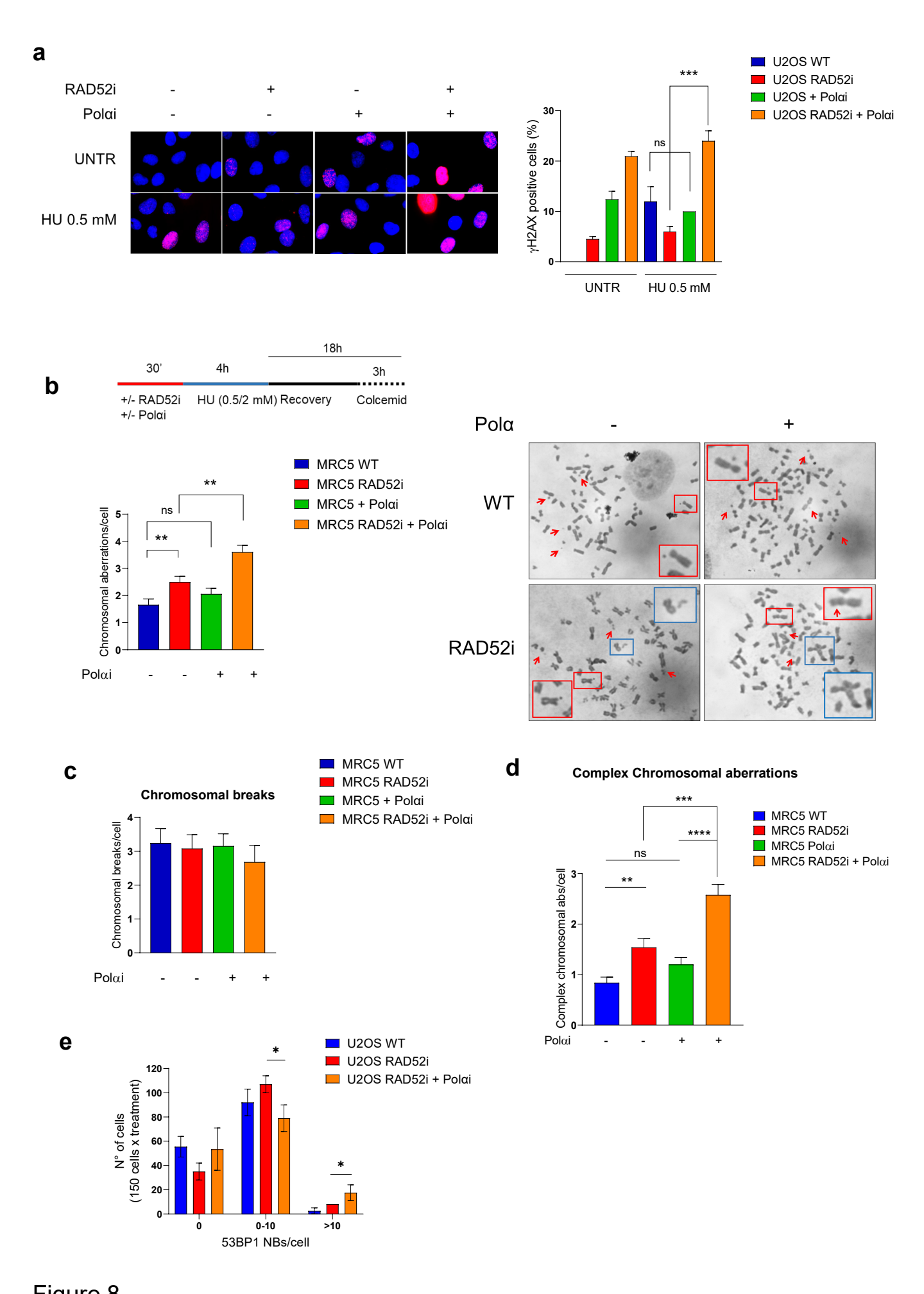
a
RAD52i
Polαi
UNTR
HU 0.5 mM
U2OS WT
U2OS RAD52i
U2OS + Polαi
U2OS RAD52i + Polαi
γH2AX positive cells (%)
***
ns
UNTR
HU 0.5 mM
b
30'
4h
18h
3h
+/- RAD52i
+/- Polαi
HU (0.5/2 mM)
Recovery
Colcemid
MRC5 WT
MRC5 RAD52i
MRC5 + Polαi
MRC5 RAD52i + Polαi
Chromosomal aberrations/cell
**
ns
Polαi
Polα
WT
RAD52i
c
Chromosomal breaks
Chromosomal breaks/cell
d
Complex Chromosomal aberrations
Complex chromosomal abs/cell
****
e
N° of cells
(150 cells x treatment)
53BP1 NBs/cell
0
0-10
>10

Figure 8

f

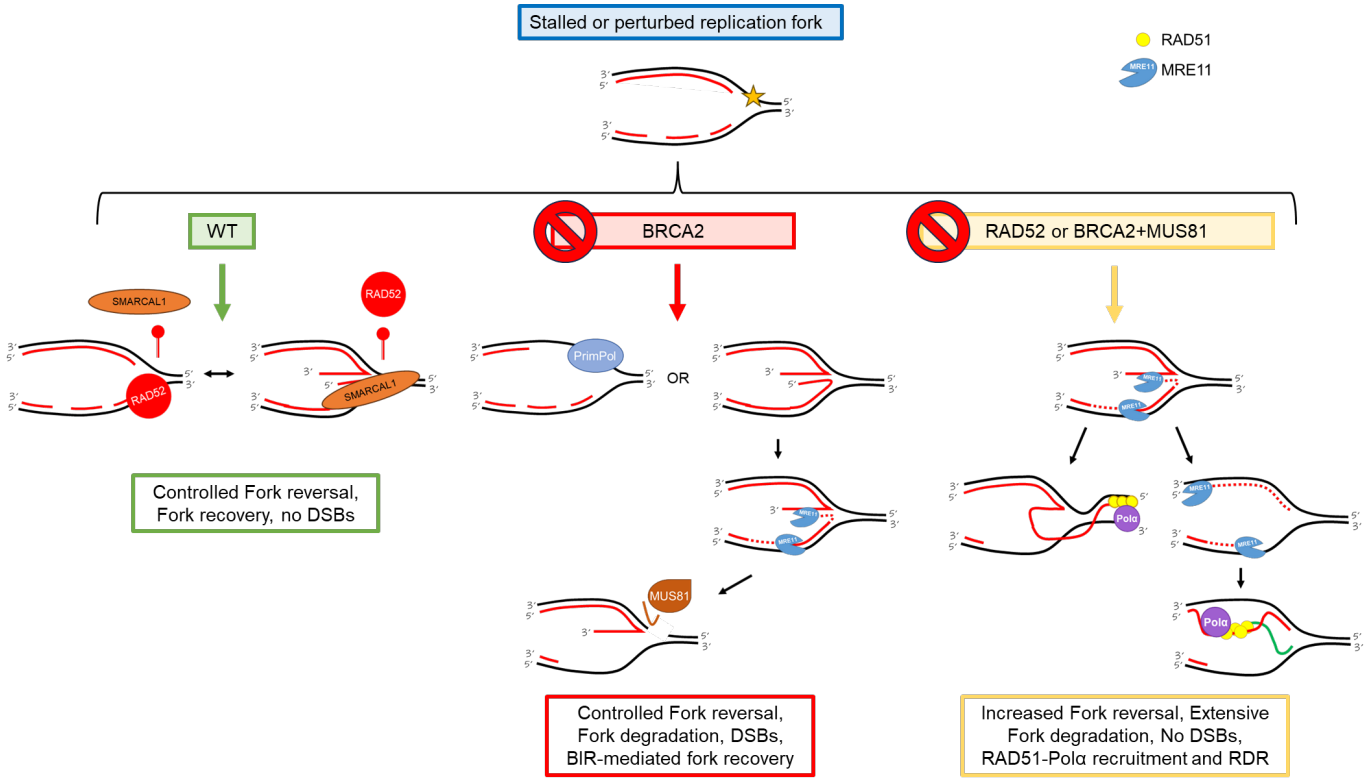

Figure 8 cont'd